J. Fluid Mech. (2021), *vol*. 927, A3, doi:10.1017/jfm.2021.729

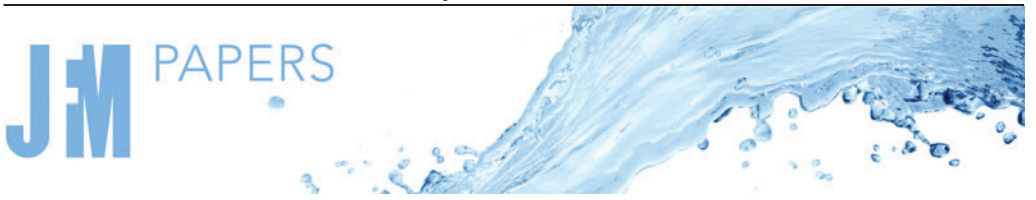

Boundary integrals for oscillating bodies in stratified fluids

Bruno Voisin†

Laboratoire des Écoulements Géophysiques et Industriels, Université Grenoble Alpes, CNRS, Grenoble INP, 38000 Grenoble, France

(Received 16 October 2020; revised 25 July 2021; accepted 15 August 2021)

The theoretical foundations of the boundary integral method are considered for inviscid monochromatic internal waves, and an analytical approach is presented for the solution of the boundary integral equation for oscillating bodies of simple shape: an elliptic cylinder in two dimensions, and a spheroid in three dimensions. The method combines the coordinate stretching introduced by Bryan and Hurley in the frequency range of evanescent waves, with analytic continuation to the range of propagating waves by Lighthill's radiation condition. Not only are the waves obtained for arbitrary oscillations of the body, with application to radial pulsations and rigid vibrations, but also the distribution of singularities equivalent to the body, allowing later inclusion of viscosity in the theory. Both a direct representation of the body as a Kirchhoff–Helmholtz integral involving single and double layers together, and an indirect representation involving a single layer alone, are considered. The indirect representation is seen to require a certain degree of symmetry of the body with respect to the horizontal and the vertical. As the surface of the body is approached the single- and double-layer potentials exhibit the same discontinuities as in classical potential theory.

Key words: internal waves, stratified flows

1. Introduction

Internal gravity waves in density-stratified fluids, inertial waves in rotating fluids and inertia–gravity waves in rotating stratified fluids, all share a common pattern under localized monochromatic excitation: a St Andrew's cross in two dimensions, and a double cone in three dimensions. The first experimental studies of this pattern used oscillating bodies to generate the waves, such as a circular cylinder (Mowbray & Rarity 1967) and a sphere (McLaren *et al.* 1973). The first theoretical studies were modelled after these experiments, and considered cylinders either circular (Hurley 1972; Appleby & Crighton

† Email address for correspondence: bruno.voisin@univ-grenoble-alpes.fr

1986) or elliptic (Hurley 1997; Hurley & Hood 2001), and spheres (Hendershott 1969; Appleby & Crighton 1987; Voisin 1991; Rieutord, Georgeot & Valdetarro 2001; Davis 2012) or spheroids (Krishna & Sarma 1969; Sarma & Krishna 1972; Lai & Lee 1981). The free oscillations of a sphere, displaced from its neutral buoyancy level then released, were also considered (Larsen 1969).

The theory combined coordinate stretching and analytic continuation; an equivalent formulation involving the Laplace transform for impulsively started oscillations was also used. The problem was solved first in the frequency range where the waves are evanescent and their equation elliptic, by stretching the coordinates so as to turn the wave equation into the Laplace equation when the Boussinesq approximation is made, and a Helmholtz equation otherwise; the solution was then continued analytically to the frequency range where the waves are propagating and their equation hyperbolic, based on the causality requirement that, for time dependence as $\exp(-\mathrm{i}\omega t)$ say, with t the time and ω the frequency, the solution be analytic in the upper half of the complex ω-plane.

Several origins have been invoked for this approach: Hendershott (1969) traced it back to Stewartson (1952), for the formation of Taylor columns; Appleby & Crighton (1986) traced it back to Hurley (1972), who combined it with conformal mapping to devise a general approach of two-dimensional monochromatic internal waves; and Voisin (1991) traced it back to Pierce (1963), for the Green's function of acoustic–gravity waves. But Rieutord *et al.* (2001) pointed out that the approach is actually much older, having been introduced first by Bryan (1889) for the determination of the inertial modes of a rotating spheroid, a problem to which it is still applied to this day (Rieutord & Noui 1999; Ivers, Jackson & Winch 2015; Backus & Rieutord 2017).

As pointed out by Ermanyuk (2002), the approach also allows the determination of the added mass of a rigid body oscillating in a stratified fluid, based on the added mass of the stretched version of the same body oscillating in a homogeneous fluid. The outcome has been compared with experiment for a spheroid (Ermanyuk 2002), a sphere (Ermanyuk & Gavrilov 2003), a cylinder with diamond-shaped (Ermanyuk & Gavrilov 2002) or circular (Brouzet *et al.* 2017) cross-section, a vertical plate and a flat-topped hill (Brouzet *et al.* 2017).

In nature, the main manifestation of monochromatic internal waves is the internal or baroclinic tide, generated in the ocean by the oscillation of the barotropic tide over bottom topography. The necessity of dealing with arbitrary topography has led to the development of a variety of theoretical approaches (Garrett & Kunze 2007). Among them is the boundary integral method, and its numerical implementation the boundary element method. The forcing, typically a free-slip condition at a solid boundary, is replaced by a distribution of singularities on the boundary. The waves are expressed as the convolution of the distribution with the Green's function of the problem, and the boundary condition is reduced to an integral equation for the distribution. Once the distribution is known, the waves are obtained immediately in the whole fluid domain.

The boundary integral method is not specific to internal waves, or even to fluid mechanics. A review of its early history has been given by Cheng & Cheng (2005), and a recent review with extensive bibliography by Martin (2006, chapter 5). The numerical development of the method dates back to the 1960s, and the method is now used routinely for Stokes flow (Pozrikidis 1992), potential flow (Pozrikidis 2002) and acoustic waves (Crighton *et al.* 1992, chapter 10), having reached the status of textbook topic (Hinch 2020, chapter 12). It is also commonly used in elasticity, heat transfer and electromagnetism; see, among many others, Brebbia, Telles & Wrobel (1984), Gaul, Kögl & Wagner (2003) and Gibson (2014).

For internal and inertial waves, the boundary integral method has been introduced first for the diffraction at a horizontal strip (Barcilon & Bleistein 1969), a vertical strip (Robinson 1969), a wedge (Hurley 1970; Robinson 1970) and a shelf break (Hurley 1972). It was not pursued further in the Western literature at the time. In Russia, however, the derivation of Kirchhoff–Helmholtz integrals by Sobolev (1954) for inertial waves and Miropol'skii (1978) for internal waves, originally to solve the initial-value problem, led to investigation of the application of the same integrals to the boundary-value problem. This was done by Kapitonov (1980) and Skazka (1981) for inertial waves in three and two dimensions, respectively, Gabov & Shevtsov (1983, 1984) for Boussinesq internal waves in three and two dimensions, respectively, and Gabov & Orazov (1986) for non-Boussinesq internal waves in one dimension, Pletner (1991) and Sundukova (1991) in three dimensions and Pletner (1992) and Allakhverdiev & Pletner (1993) in two dimensions.

A long series of papers followed, initiated by Gabov and continued by his collaborators after his death in 1989 (Sveshnikov, Shishmarev & Pletner 1989). The series is presented in table 1, together with two separate papers by Korobkin (1990) and Davydova (2006*a*), employing the same approach. The problem was considered for impulsive switch-on, and the steady state investigated in the large-time limit. Only the first papers in the series provided explicit solutions, while the later papers focused on the existence and unicity of a solution. The papers are largely derivative, exploring small variations of a limited number of configurations. Some results were published twice, in full form in regular journals and in summary form in *Doklady*. Some papers are identical (Kharik & Pletner 1990*a*,*b*), or only differ from each other by minute details (Krutitskii 1996*a*,*d*, and also 1996*e*, 1997*b*), or adapt word-for-word an earlier study of inertia–gravity waves (Krutitskii 2000) to inertial waves (Krutitskii 2001) and internal waves (Krutitskii 2003*b*). In spite of these limitations, and because this body of work seems mostly unknown in the Western literature, it has felt useful to present it here.

Finally, three decades after its introduction for diffraction problems, the boundary integral method was brought back into the Western literature for generation problems, by Llewellyn Smith & Young (2003) for the oscillations of a vertical barrier, considered analytically, and Pétrélis, Llewellyn Smith & Young (2006) for the oscillations of several topographies, considered numerically. Further analytical application was performed by Nycander (2006) and Musgrave *et al.* (2016) to one or several vertical barriers, and further numerical application by Balmforth & Peacock (2009), Echeverri & Peacock (2010) and Echeverri *et al.* (2011) to a variety of topographies. The scattering at a Gaussian topography was also considered numerically by Mathur, Carter & Peacock (2014). The mathematical foundations of the method, for both generation and scattering, were discussed by Martin & Llewellyn Smith (2012).

In parallel, Sturova applied the boundary integral method to the oscillations of circular or elliptic horizontal cylinders, both analytically (2001) and numerically (2006, 2011), while Davydova & Chashechkin (2004) and Davydova (2004, 2006*b*) discussed how the method can be combined with multiple scale analysis to calculate the waves and boundary layer generated by the oscillations of a vertical cylinder of arbitrary cross section in a slightly viscous fluid.

The aim of the present paper is twofold: first, to show how the method of coordinate stretching and analytic continuation can be combined with the boundary integral method, to solve the problem of internal wave generation by an oscillating body in an inviscid fluid; and second, to investigate the peculiarities of boundary integrals for monochromatic internal waves, compared with their usual properties for the Laplace and Helmholtz equations.

		Single source	Multiple sources
2D	Horizontal segment	Gabov (1985) Gabov & Krutitskii (1989)	
	Inclined segment	Gabov (1984*a*) Gabov & Pletner (1985, 1987*a*) Pletner (1988) Kharik (1993) Krutitskii (1996*e*, 1997*b*)	Krutitskii (1992*a*,*b*, 1994, 1995, 1996*b*, 1997*c*)
	Vertical segment	Gabov & Krutitskii (1987) Krutitskii (1988) Korobkin (1990)	
	Arbitrary curve	Gabov (1984*b*) Gabov & Pletner (1987*b*,*c*) Kharik & Pletner (1990*a*,*b*)	Krutitskii (1996*a*,*c*,*d*, 1997*a*, 1998, 2003*a*)
3D	Horizontal disk	Gabov & Pletner (1988) Pletner & Tverskaya (1989, 1991) Pletner (1990*a*,*b*)	
	Arbitrary horizontal domain	Gabov & Simakov (1989) Simakov (1989)	
	Vertical cylinder	Davydova (2006*a*)	
	Arbitrary surface		Krutitskii (2000, 2001, 2003*b*)
NB	Arbitrary curve	Korpusov, Pletner & Sveshnikov (1997*a*,*b*,*c*)	Korpusov, Pletner & Sveshnikov (1998)

Table 1. Publications based on the work of S.A. Gabov on the boundary integral method for internal and/or inertial waves, in two dimensions (2D) or three dimensions (3D). Unless stated otherwise (NB), the Boussinesq approximation is made throughout.

Boundary integrals have been considered by Martin & Llewellyn Smith (2012) already. We focus accordingly on two aspects complementary to their investigations: the equivalence (or lack thereof) between a direct formulation based on a Kirchhoff–Helmholtz integral involving both single and double layers, and indirect formulations based on single or double layers alone; and the discontinuities of the boundary integrals at the boundary.

The derivation of the waves is accompanied by that of a distribution of singularities equivalent to the body, with two consequences. First, once the spatial spectrum of the distribution is known, additional phenomena, like viscosity and unsteadiness, that affect the propagation of the waves and set their local structure, can be added into the analysis; this approach has been pioneered by Lighthill (1978, § 4.10) and Hurley & Keady (1997), and recently developed by Voisin (2020). Second, for a rigid body, the added mass of the body follows directly from the first moment of the distribution, providing immediate access to the radiated energy (called 'conversion rate' within the context of internal tides) and to the forces exerted on the body, without requiring the actual calculation of the waves; this aspect will be reported separately, and has been presented in summary form by Voisin (2009).

The problem of internal wave generation by an oscillating body is stated in § 2 and its direct formulation as a boundary integral in § 3. It is solved in §§ 4 and 5 for an elliptic cylinder and a spheroid, as prototypal two- and three-dimensional bodies, respectively.

Arbitrary oscillations are considered first, and the results applied to the two simplest types of oscillations: radial pulsations and rigid vibrations. The indirect formulation of the problem as a single-layer integral is presented in § 6 and shown to lead to a simple representation of the body. The representations of a vibrating sphere in Voisin, Ermanyuk & Flór (2011) and a vibrating elliptic cylinder in Voisin (2020) are recovered as particular cases. Sections 7 and 8 discuss the behaviour of the boundary integrals at the boundary and in the far field, respectively. They are followed by a conclusion in § 9.

2. Statement of the problem

We consider linear internal waves in an inviscid uniformly stratified Boussinesq fluid of buoyancy frequency N, and use the generalized potential introduced by Sobolev (1954) for inertial waves and Gorodtsov & Teodorovich (1980), Hart (1981), Gray, Hart & Farrell (1983), Gabov & Mamedov (1983), Gabov, Malysheva & Sveshnikov (1983), Gabov *et al.* (1984), Voisin (1991, 2003) and Gorodtsov (2013) for internal waves, with specifics listed in table 2. Gauge invariance, ensuring the completeness of the representation, has been discussed by Sobolev (1954), Gray *et al.* (1983) and Gabov *et al.* (1983). A different but related representation based on the toroidal/poloidal decomposition has been introduced by Kistovich & Chashechkin (2001). Denoting the potential, called 'internal' by Voisin (1991), as ψ, the wave equation takes the form

$$\left(\frac{\partial^2}{\partial t^2}\nabla^2 + N^2\nabla_h^2\right)\psi = q, \tag{2.1}$$

with z the vertical coordinate, $\boldsymbol{x} = (x, y, z)$ the position, $\boldsymbol{\nabla} = (\partial/\partial x, \partial/\partial y, \partial/\partial z)$ the del operator and $\boldsymbol{\nabla}_h = (\partial/\partial x, \partial/\partial y, 0)$ its horizontal projection. The forcing is represented as a source of mass releasing the volume $q = \boldsymbol{\nabla}\cdot\boldsymbol{u}$ of fluid per unit volume per unit time. The disturbances $\boldsymbol{u}$ in velocity, p in pressure and ρ in density are expressed in terms of ψ as

$$\boldsymbol{u} = \left(\frac{\partial^2}{\partial t^2}\boldsymbol{\nabla} + N^2\boldsymbol{\nabla}_h\right)\psi, \quad p = -\rho_0\left(\frac{\partial^2}{\partial t^2} + N^2\right)\frac{\partial}{\partial t}\psi, \quad \rho = \rho_0\frac{N^2}{g}\frac{\partial^2}{\partial t\partial z}\psi, \tag{2.2a–c}$$

with ρ_0 the density at rest and g the acceleration due to gravity.

We are interested in monochromatic waves of frequency ω, varying in time through the factor $\exp(-\mathrm{i}\omega t)$ which is suppressed in the following. The wave equation becomes

$$(N^2\nabla_h^2 - \omega^2\nabla^2)\psi = q, \tag{2.3}$$

and the fluid dynamical quantities become

$$\boldsymbol{u} = (N^2\boldsymbol{\nabla}_h - \omega^2\boldsymbol{\nabla})\psi, \quad p = \mathrm{i}\rho_0\omega(N^2 - \omega^2)\psi, \quad \rho = -\mathrm{i}\rho_0\omega\frac{N^2}{g}\frac{\partial}{\partial z}\psi. \tag{2.4a–c}$$

An oscillating body of surface S and outward normal $\boldsymbol{n}$ generates waves by imposing a normal velocity U_n at S, through the free-slip boundary condition

$$\boldsymbol{n}\cdot\boldsymbol{u} = U_n \quad (\boldsymbol{x}\in S). \tag{2.5}$$

The boundary integral method replaces this condition by a source term q in the wave equation.

	Rotation	Stratif.	Viscosity	Non-Bouss.	Compress.	Heat cond.
Sobolev (1954)	×					
Gorodtsov & Teodorovich (1980)		×				
Hart (1981)	×		×			
		×	×			
Gray *et al.* (1983)		×				
Gabov & Mamedov (1983)		×		×		
Gabov *et al.* (1983)		×			×	
Gabov *et al.* (1984)	×	×			×	
Voisin (1991)		×		×		
Voisin (2003)		×	×			
Gorodtsov (2013)		×		×		
		×	×			×

Table 2. Introduction of generalized potentials for waves in rotating and/or stratified fluids with or without viscosity, non-Boussinesq effects, compressibility and heat conduction.

3. Direct approach

3.1. *Kirchhoff–Helmholtz integral*

For this, we adapt the approach used for the Laplace and Helmholtz equations; see, for example, Lighthill (1986, § 8.1), Jackson (1999, § 1.8), Martin (2006, § 5.6) and Pierce (2019, § 4.6). For two arbitrary functions f and g we write

$$f(N^2\nabla_h^2-\omega^2\nabla^2)g-g(N^2\nabla_h^2-\omega^2\nabla^2)f=\boldsymbol{\nabla}\cdot[f(N^2\boldsymbol{\nabla}_h-\omega^2\boldsymbol{\nabla})g-g(N^2\boldsymbol{\nabla}_h-\omega^2\boldsymbol{\nabla})f], \tag{3.1}$$

which upon integration inside a volume V delimited by the surface S of outward normal $\boldsymbol{n}$, and application of the divergence theorem, gives

$$\begin{aligned}&\int_V [f(N^2\nabla_h^2-\omega^2\nabla^2)g-g(N^2\nabla_h^2-\omega^2\nabla^2)f]\,\mathrm{d}^3x\\&\quad=\int_S\left[f\left(N^2\frac{\partial}{\partial n_h}-\omega^2\frac{\partial}{\partial n}\right)g-g\left(N^2\frac{\partial}{\partial n_h}-\omega^2\frac{\partial}{\partial n}\right)f\right]\mathrm{d}^2S,\end{aligned} \tag{3.2}$$

where $\partial/\partial n=\boldsymbol{n}\cdot\boldsymbol{\nabla}$ and $\partial/\partial n_h=\boldsymbol{n}\cdot\boldsymbol{\nabla}_h$.

We apply this Green's theorem to the volume V_+ exterior to the oscillating body, delimited internally by the surface S of the body (with outward normal $-\boldsymbol{n}$) and externally by a surface S_∞ at infinity, as shown in figure 1. The volume interior to the body is denoted as V_-. We choose a fixed observation point $\boldsymbol{x}$ in either V_+ or V_-, and denote the variable integration point in V_+ as $\boldsymbol{x}'$. We take for f the internal potential $\psi(\boldsymbol{x}')$ at $\boldsymbol{x}'$, and for g the propagator $G(\boldsymbol{x}-\boldsymbol{x}')$ from $\boldsymbol{x}'$ to $\boldsymbol{x}$. Here, G is the Green's function of the wave equation, corresponding to unit point forcing and satisfying

$$(N^2\nabla_h^2-\omega^2\nabla^2)G(\boldsymbol{x})=\delta(\boldsymbol{x}), \tag{3.3}$$

with δ the Dirac delta function, together with the causality condition that G be analytic in the upper half of the complex ω-plane. We assume that both G and ψ decay fast enough at infinity for the contribution of S_∞ to vanish, and will come back to this assumption later

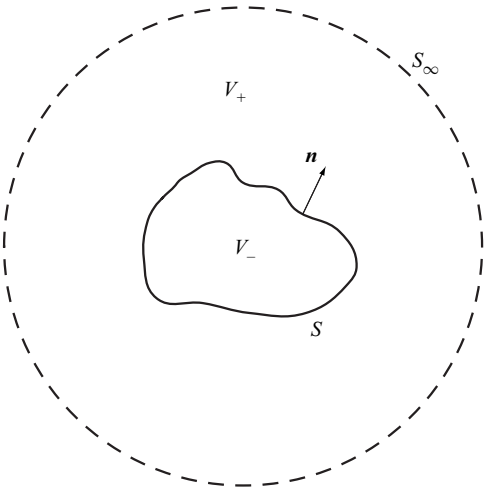

Figure 1. Surfaces for the derivation of the Kirchhoff–Helmholtz integral.

in § 8. We obtain the Kirchhoff–Helmholtz integral

$$\int_S \left[G(\boldsymbol{x}-\boldsymbol{x}') \left(N^2 \frac{\partial}{\partial n'_h} - \omega^2 \frac{\partial}{\partial n'} \right) \psi(\boldsymbol{x}') - \psi(\boldsymbol{x}') \left(N^2 \frac{\partial}{\partial n'_h} - \omega^2 \frac{\partial}{\partial n'} \right) G(\boldsymbol{x}-\boldsymbol{x}') \right] \mathrm{d}^2 S'$$

$$= \psi(\boldsymbol{x}) \quad (\boldsymbol{x} \in V_+), \tag{3.4a}$$

$$= 0 \quad (\boldsymbol{x} \in V_-), \tag{3.4b}$$

where $\partial/\partial n' = \boldsymbol{n}' \cdot \boldsymbol{\nabla}'$ and $\partial/\partial n'_h = \boldsymbol{n}' \cdot \boldsymbol{\nabla}'_h$, with $\boldsymbol{n}' = \boldsymbol{n}(\boldsymbol{x}')$.

Letting now $\boldsymbol{x}$ approach S from within V_+, we obtain

$$\Psi(\boldsymbol{x}) + \int_S \Psi(\boldsymbol{x}') \left(N^2 \frac{\partial}{\partial n'_h} - \omega^2 \frac{\partial}{\partial n'} \right) G(\boldsymbol{x}-\boldsymbol{x}') \, \mathrm{d}^2 S' = \int_S U_n(\boldsymbol{x}') G(\boldsymbol{x}-\boldsymbol{x}') \, \mathrm{d}^2 S', \tag{3.5}$$

an integral relation between the surface values Ψ of the internal potential (hence the pressure) and U_n of the normal velocity, to be satisfied for all $\boldsymbol{x}$ on the outer side S_+ of S. Given the pressure this provides an integral equation of the first kind for the velocity, and given the velocity an equation of the second kind for the pressure. Once it is solved, the waves are expressed through the fluid, for $\boldsymbol{x} \in V_+$, as

$$\psi(\boldsymbol{x}) = \int_S \left[U_n(\boldsymbol{x}') G(\boldsymbol{x}-\boldsymbol{x}') - \Psi(\boldsymbol{x}') \left(N^2 \frac{\partial}{\partial n'_h} - \omega^2 \frac{\partial}{\partial n'} \right) G(\boldsymbol{x}-\boldsymbol{x}') \right] \mathrm{d}^2 S'. \tag{3.6}$$

This expression combines two terms: a single-layer potential

$$\psi_s(\boldsymbol{x}) = \int_S \sigma(\boldsymbol{x}') G(\boldsymbol{x}-\boldsymbol{x}') \, \mathrm{d}^2 S', \tag{3.7}$$

generated by the surface distribution of monopoles

$$q_s(\boldsymbol{x}) = \sigma(\boldsymbol{x}) \delta_S(\boldsymbol{x}), \tag{3.8}$$

with density

$$\sigma(\boldsymbol{x}) = U_n(\boldsymbol{x}), \tag{3.9}$$

where δ_S is the Dirac delta function of support S, such that, if $S(\boldsymbol{x}) = 0$ is the equation of the surface, $\delta_S(\boldsymbol{x}) = |\boldsymbol{\nabla} S|\delta[S(\boldsymbol{x})]$; and a double-layer potential

$$\psi_d(\boldsymbol{x}) = \int_S \mu(\boldsymbol{x}') \left(N^2 \frac{\partial}{\partial n'_h} - \omega^2 \frac{\partial}{\partial n'} \right) G(\boldsymbol{x} - \boldsymbol{x}') \, \mathrm{d}^2 S', \tag{3.10}$$

generated by the surface distribution of dipoles

$$q_d(\boldsymbol{x}) = - \left(N^2 \frac{\partial}{\partial n_h} - \omega^2 \frac{\partial}{\partial n} \right) [\mu(\boldsymbol{x}) \delta_S(\boldsymbol{x})], \tag{3.11}$$

with density

$$\mu(\boldsymbol{x}) = -\Psi(\boldsymbol{x}). \tag{3.12}$$

See, for example, Jackson (1999, § 1.6) for the introduction of such potentials in electrostatics, and Martin (2006, § 5.3) for non-dispersive waves.

The forcing is thus represented by the equivalent source

$$q(\boldsymbol{x}) = U_n(\boldsymbol{x}) \delta_S(\boldsymbol{x}) + \left(N^2 \frac{\partial}{\partial n_h} - \omega^2 \frac{\partial}{\partial n} \right) [\Psi(\boldsymbol{x}) \delta_S(\boldsymbol{x})]. \tag{3.13}$$

Such representation allows the extension of (3.6) to a viscous fluid, once the spectrum

$$q(\boldsymbol{k}) = \int q(\boldsymbol{x}) \exp(-\mathrm{i}\boldsymbol{k} \cdot \boldsymbol{x}) \, \mathrm{d}^3 x \tag{3.14}$$

is known, namely

$$q(\boldsymbol{k}) = \int_S [U_n(\boldsymbol{x}) + \mathrm{i}\boldsymbol{n} \cdot (N^2 \boldsymbol{k}_h - \omega^2 \boldsymbol{k}) \Psi(\boldsymbol{x})] \exp(-\mathrm{i}\boldsymbol{k} \cdot \boldsymbol{x}) \, \mathrm{d}^2 S, \tag{3.15}$$

with $\boldsymbol{k}$ the wave vector and $\boldsymbol{k}_h$ its horizontal projection. The extension follows the lines laid by Lighthill (1978, § 4.10), Hurley & Keady (1997) and Voisin (2020); it will be discussed further in § 6.2.

3.2. *Green's function*

To determine the Green's function we use the technique introduced by Bryan (1889) for inertial waves and Hurley (1972) for internal waves. In the frequency range $\omega > N$ of evanescent waves, (3.3), rewritten as

$$\left[(\omega^2 - N^2) \frac{\partial^2}{\partial x^2} + (\omega^2 - N^2) \frac{\partial^2}{\partial y^2} + \omega^2 \frac{\partial^2}{\partial z^2} \right] G(\boldsymbol{x}) = -\delta(\boldsymbol{x}), \tag{3.16}$$

is elliptic. Stretching the coordinates according to

$$x_\star = \frac{\omega}{N} x, \quad y_\star = \frac{\omega}{N} y, \quad z_\star = \left(\frac{\omega^2}{N^2} - 1 \right)^{1/2} z \tag{3.17a–c}$$

transforms it into a Poisson equation, of known Green's function (Bleistein 1984, § 6.2). Causality allows the continuation of the solution to the frequency range $0 < \omega < N$ of propagating waves. Continuation is implemented via Lighthill's (1978, § 4.9) radiation

condition, namely by adding to the frequency a small positive imaginary part ϵ which is later allowed to tend to 0; in other words, by performing the replacement

$$\omega \to \omega + \mathrm{i}0 = \lim_{\epsilon \to 0_+} (\omega + \mathrm{i}\epsilon). \tag{3.18}$$

The Green's function is obtained in three dimensions as

$$G(\boldsymbol{x}) = \frac{1}{4\pi N(\omega^2 - N^2)^{1/2}|\boldsymbol{x}_\star|}, \tag{3.19}$$

that is in unstretched coordinates

$$G(\boldsymbol{x}) = \frac{1}{4\pi(\omega^2 - N^2)^{1/2}(\omega^2 r^2 - N^2 z^2)^{1/2}}, \tag{3.20}$$

with associated velocity

$$\boldsymbol{u}_G(\boldsymbol{x}) = (N^2\boldsymbol{\nabla}_h - \omega^2\boldsymbol{\nabla})G = \frac{\omega^2(\omega^2 - N^2)^{1/2}\boldsymbol{x}}{4\pi(\omega^2 r^2 - N^2 z^2)^{3/2}}. \tag{3.21}$$

Similarly, in two dimensions, when the waves are independent of the horizontal coordinate y, the Green's function is

$$G(\boldsymbol{x}) = -\frac{\ln|\boldsymbol{x}_\star|}{2\pi\omega(\omega^2 - N^2)^{1/2}}. \tag{3.22}$$

Knowing the Green's function we can now solve (3.5) for prototypal oscillating bodies, namely an elliptic cylinder in two dimensions and a spheroid in three dimensions, in the next two sections.

4. Elliptic cylinder

An elliptic cylinder of horizontal semi-axis a, vertical semi-axis b and equation

$$\frac{x^2}{a^2} + \frac{z^2}{b^2} = 1, \tag{4.1}$$

is transformed by the stretching (3.17) into another elliptic cylinder, of semi-axes

$$a_\star = \frac{\omega}{N}a, \quad b_\star = \left(\frac{\omega^2}{N^2} - 1\right)^{1/2} b, \tag{4.2a,b}$$

respectively. For $(a/b)^2 + (N/\omega)^2 > 1$, corresponding to an original ellipse which either has its major axis horizontal and operates at any frequency $\omega > N$, or has its major axis vertical and operates in the frequency range $N < \omega < N/[1 - (a/b)^2]^{1/2}$, the stretched ellipse has its major axis horizontal. We consider this situation first, and will deal with the other situations by analytic continuation.

4.1. *Solution for $\omega > N$ and $(a/b)^2 + (N/\omega)^2 > 1$*

For $(a/b)^2 + (N/\omega)^2 > 1$, the stretched ellipse has its foci along the horizontal axis, at $(x_\star = \pm c, z_\star = 0)$, with

$$c = (a_\star^2 - b_\star^2)^{1/2} = \left[\frac{\omega^2}{N^2}a^2 + \left(1 - \frac{\omega^2}{N^2}\right)b^2\right]^{1/2}. \tag{4.3}$$

We introduce elliptic coordinates (ξ, η) defined by

$$x_\star = c\cosh\xi\cos\eta, \quad z_\star = c\sinh\xi\sin\eta, \tag{4.4a,b}$$

with $0 \leqslant \xi < \infty$ and $0 \leqslant \eta < 2\pi$. This definition is inverted in terms of the distances to the foci,

$$r_\pm = [(x_\star \pm c)^2 + z_\star^2]^{1/2} = c(\cosh\xi \pm \cos\eta), \tag{4.5}$$

as

$$\cosh\xi = \frac{r_+ + r_-}{2c}, \quad \cos\eta = \frac{r_+ - r_-}{2c}; \tag{4.6a,b}$$

see Happel & Brenner (1983, Appendix A) or Landau & Lifshitz (1984, § 4). The spatial derivatives become

$$c\frac{\partial}{\partial x_\star} = \frac{1}{\sinh^2\xi + \sin^2\eta}\left(\sinh\xi\cos\eta\frac{\partial}{\partial\xi} - \cosh\xi\sin\eta\frac{\partial}{\partial\eta}\right), \tag{4.7a}$$

$$c\frac{\partial}{\partial z_\star} = \frac{1}{\sinh^2\xi + \sin^2\eta}\left(\cosh\xi\sin\eta\frac{\partial}{\partial\xi} + \sinh\xi\cos\eta\frac{\partial}{\partial\eta}\right), \tag{4.7b}$$

where $\sinh^2\xi + \sin^2\eta = \sinh(\xi + \mathrm{i}\eta)\sinh(\xi - \mathrm{i}\eta)$.

At the ellipse, $\xi = \xi_0$ with

$$a_\star = c\cosh\xi_0, \quad b_\star = c\sinh\xi_0, \tag{4.8a,b}$$

so that

$$\xi_0 = \operatorname{arctanh}\left(\frac{b_\star}{a_\star}\right) = \operatorname{arctanh}\left[\frac{b}{a}\left(1 - \frac{N^2}{\omega^2}\right)^{1/2}\right]. \tag{4.9}$$

There, η reduces to the eccentric angle for the original ellipse, such that

$$x = a\cos\eta, \quad z = b\sin\eta; \tag{4.10a,b}$$

see Sommerville (1933, § IV.10) or Milne-Thomson (1968, § 6.32). The arc length element follows as

$$\mathrm{d}l = (a^2\sin^2\eta + b^2\cos^2\eta)^{1/2}\,\mathrm{d}\eta, \tag{4.11}$$

and the outward normal as

$$\boldsymbol{n} = \frac{b\boldsymbol{e}_x\cos\eta + a\boldsymbol{e}_z\sin\eta}{(a^2\sin^2\eta + b^2\cos^2\eta)^{1/2}}, \tag{4.12}$$

where $\boldsymbol{e}_x$ and $\boldsymbol{e}_z$ are unit vectors along the x- and z-axes, respectively. The boundary integral equation (3.5) becomes

$$2\pi\Psi(\eta) + \int_0^{2\pi}\left[\Psi(\eta')\frac{\partial}{\partial\xi'} + \frac{(a^2\sin^2\eta' + b^2\cos^2\eta')^{1/2}}{\omega(\omega^2 - N^2)^{1/2}}U_n(\eta')\right]\ln|\boldsymbol{x}_\star - \boldsymbol{x}_\star'|\,\mathrm{d}\eta' = 0, \tag{4.13}$$

where $\xi = \xi_0 + 0 > \xi' = \xi_0$.

To solve it, we adapt the procedure used by Gorodtsov & Teodorovich (1982) for the potential flow around a circular cylinder. The normal velocity $U_n(\eta)$ is expanded in circular functions as

$$(a^2\sin^2\eta + b^2\cos^2\eta)^{1/2}U_n(\eta) = c\sum_{m=0}^{\infty}[U_m^{(\mathrm{c})}\cos(m\eta) + U_m^{(\mathrm{s})}\sin(m\eta)], \tag{4.14}$$

with

$$cU_m^{(\mathrm{c,s})} = \frac{\epsilon_m}{2\pi}\int_0^{2\pi}(a^2\sin^2\eta + b^2\cos^2\eta)^{1/2}U_n(\eta)(\cos,\sin)(m\eta)\,\mathrm{d}\eta, \tag{4.15}$$

and the surface potential $\Psi(\eta)$ as

$$\Psi(\eta) = \sum_{m=0}^{\infty}[\Psi_m^{(\mathrm{c})}\cos(m\eta) + \Psi_m^{(\mathrm{s})}\sin(m\eta)], \tag{4.16}$$

with

$$\Psi_m^{(\mathrm{c,s})} = \frac{\epsilon_m}{2\pi}\int_0^{2\pi}\Psi(\eta)(\cos,\sin)(m\eta)\,\mathrm{d}\eta. \tag{4.17}$$

Here, $\epsilon_m = 1$ for $m = 0$ and 2 for $m \geqslant 1$ is the Neumann factor. The Green's function has been shown by Morse & Feshbach (1953, p. 1202) to admit of the expansion

$$\ln|\boldsymbol{x}_\star - \boldsymbol{x}'_\star| = \xi_> + \ln\left(\frac{c}{2}\right) - \sum_{m=1}^{\infty}\frac{2}{m}\exp(-m\xi_>)[\cosh(m\xi_<)\cos(m\eta)\cos(m\eta') + \sinh(m\xi_<)\sin(m\eta)\sin(m\eta')], \tag{4.18}$$

where $\xi_< = \min(\xi,\xi')$ and $\xi_> = \max(\xi,\xi')$. Use of these expansions turns (4.13) into a diagonal (infinite) linear system, of solution

$$\Psi_0^{(\mathrm{c})} = -\frac{c}{\omega(\omega^2 - N^2)^{1/2}}\xi_0 U_0^{(\mathrm{c})}, \quad \Psi_0^{(\mathrm{s})} = 0, \tag{4.19a}$$

$$\Psi_m^{(\mathrm{c,s})} = \frac{c}{\omega(\omega^2 - N^2)^{1/2}}\frac{U_m^{(\mathrm{c,s})}}{m} \quad (m \neq 0). \tag{4.19b}$$

Evaluation of the convolution integral (3.6), followed by differentiation according to (2.4), yields

$$p = \mathrm{i}\rho_0 c(\omega^2 - N^2)^{1/2}\left\{U_0^{(\mathrm{c})}\xi - \frac{1}{2}\sum_{\pm}\sum_{m=1}^{\infty}[U_m^{(\mathrm{c})} \pm \mathrm{i}U_m^{(\mathrm{s})}]\frac{\exp[-m(\xi - \xi_0 \pm \mathrm{i}\eta)]}{m}\right\} \tag{4.20}$$

for the pressure, and

$$\boldsymbol{u} = \frac{1}{2}\sum_{\pm}\frac{(\omega^2 - N^2)^{1/2}\boldsymbol{e}_x \pm \mathrm{i}\omega\boldsymbol{e}_z}{N\sinh(\xi \pm \mathrm{i}\eta)}\sum_{m=0}^{\infty}[U_m^{(\mathrm{c})} \pm \mathrm{i}U_m^{(\mathrm{s})}]\exp[-m(\xi - \xi_0 \pm \mathrm{i}\eta)] \tag{4.21}$$

for the velocity.

4.2. *Solution for $\omega > N$ and $(a/b)^2 + (N/\omega)^2 < 1$*

These results are continued analytically to $(a/b)^2 + (N/\omega)^2 < 1$ by applying (3.18). The stretched ellipse has its foci along the vertical axis, at $(x_\star = 0, z_\star = \pm c')$, with

$$c' = \mathrm{i}c = \left[\left(\frac{\omega^2}{N^2} - 1\right) b^2 - \frac{\omega^2}{N^2} a^2\right]^{1/2}. \tag{4.22}$$

This prompts the introduction of elliptic coordinates (ξ', η), defined by

$$x_\star = c' \sinh \xi' \cos \eta, \quad z_\star = c' \cosh \xi' \sin \eta, \tag{4.23a,b}$$

where $0 \leqslant \xi' < \infty$ and $0 \leqslant \eta < 2\pi$. Writing

$$x_\star = c \cosh\left(\xi' + \mathrm{i}\frac{\pi}{2}\right) \cos \eta, \quad z_\star = c \sinh\left(\xi' + \mathrm{i}\frac{\pi}{2}\right) \sin \eta, \tag{4.24a,b}$$

the solution of the problem is seen to follow immediately from that in § 4.1, by replacing ξ by $\xi' + \mathrm{i}\pi/2$ and c by $-\mathrm{i}c'$ throughout.

4.3. *Solution for $\omega < N$*

In the frequency range $0 < \omega < N$, the waves propagate at the angle $\theta_0 = \arccos(\omega/N)$ to the vertical. The semi-focal distance of the stretched ellipse becomes

$$c = (a^2 \cos^2 \theta_0 + b^2 \sin^2 \theta_0)^{1/2}, \tag{4.25}$$

a quantity interpreted by Hurley (1997) as the half-width of the wave beams delimited by the critical wave rays tangential to the ellipse on either side. The semi-axes become

$$a_\star = a \cos \theta_0 = c \cos \eta_0, \quad b_\star = \mathrm{i}b \sin \theta_0 = \mathrm{i}c \sin \eta_0, \tag{4.26a,b}$$

where

$$\eta_0 = \arctan\left(\frac{b}{a} \tan \theta_0\right) \tag{4.27}$$

is the eccentric angle of the critical points at which the critical rays are tangential to the ellipse. Both definitions are illustrated in figure 2.

The stretched elliptic coordinates ξ and η become complex, with ξ taking the value $\xi_0 = \mathrm{i}\eta_0$ at the ellipse. The greatest difficulty here is the expression of ξ and η in more comprehensible coordinates. For a sphere or spheroid, Sarma & Krishna (1972) expressed the associated stretched spheroidal coordinates in terms of algebraic functions of the Cartesian coordinates, but did not consider the determination of these multivalued functions explicitly. Hendershott (1969) and Voisin (1991) set the determination in the far field. Appleby & Crighton proceeded differently, for both the circular cylinder (1986) and the sphere (1987), decomposing the wave field into zones delimited by the critical rays, and investigating the properties of the stretched coordinates in each zone, concluding for the sphere that 'this illustrates the difficulty of working in more comprehensible coordinates'. Davis (2012) combined the two approaches together for the sphere, expressing, in each zone, the stretched coordinates in terms of real algebraic functions of the Cartesian coordinates.

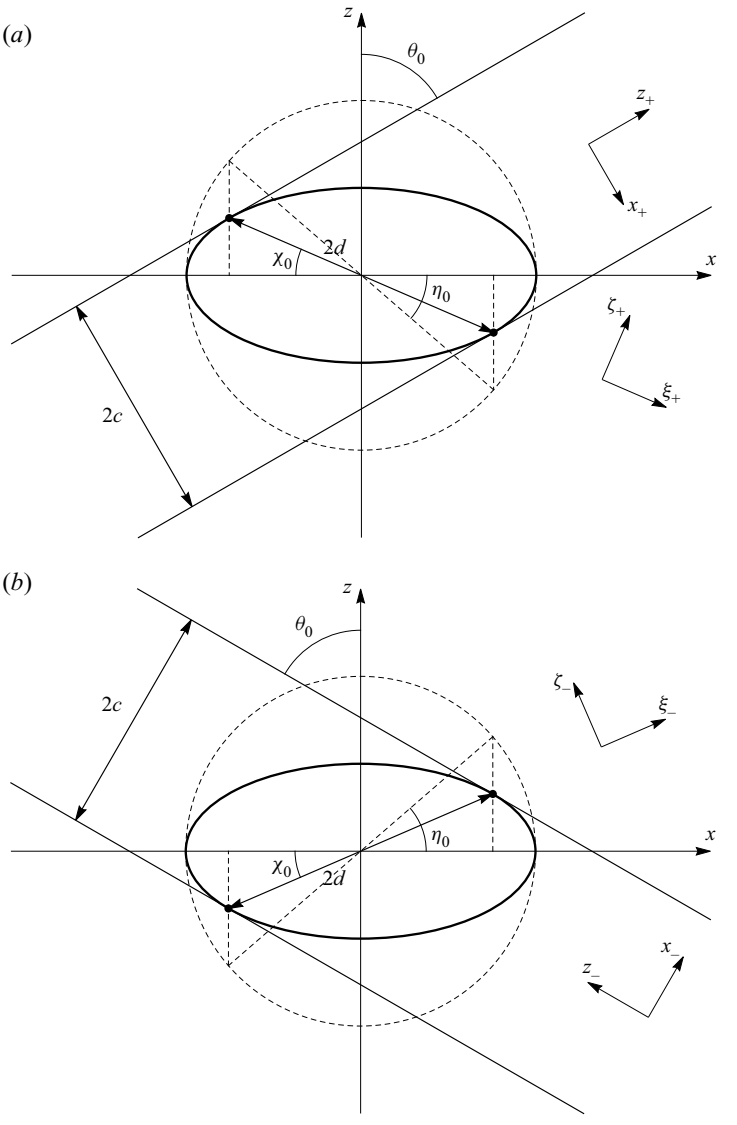

Figure 2. Geometry for the beams of waves propagating (*a*) upward to the right and downward to the left, and (*b*) downward to the right and upward to the left.

In actuality, Lighthill's radiation condition (3.18) allows both the stretched coordinates to be expressed in terms of the characteristic coordinates

$$x_\pm = x\cos\theta_0 \mp z\sin\theta_0, \quad z_\pm = \pm x\sin\theta_0 + z\cos\theta_0, \tag{4.28a,b}$$

shown in figure 2, and the associated multivalued functions to be determined unequivocally. The inversion formulae (4.5)–(4.6) are not convenient for this purpose. We proceed instead from (3.17), (4.3) and (4.4), writing

$$\cosh\xi\cos\eta = \frac{\omega x}{[\omega^2a^2 + (N^2-\omega^2)b^2]^{1/2}}, \quad \sinh\xi\sin\eta = \frac{(\omega^2-N^2)^{1/2}z}{[\omega^2a^2 + (N^2-\omega^2)b^2]^{1/2}}. \tag{4.29a,b}$$

Expanding these for $\omega = N\cos\theta_0 + \mathrm{i}\epsilon$, with $0 < \epsilon/N \ll 1$, we get

$$\cosh\xi\cos\eta \sim \frac{x}{c}\left(\cos\theta_0 + \mathrm{i}\frac{\epsilon}{N}\frac{b^2}{c^2}\right), \quad \sinh\xi\sin\eta \sim \mathrm{i}\frac{z}{c}\left(\sin\theta_0 - \mathrm{i}\frac{\epsilon}{N}\frac{a^2}{c^2}\cot\theta_0\right), \tag{4.30a,b}$$

so that

$$\cosh(\xi \pm \mathrm{i}\eta) \sim \frac{x_\pm}{c} \pm \mathrm{i}\frac{\epsilon}{N}\frac{\zeta_\pm}{c}\frac{d}{c\sin\theta_0}. \tag{4.31}$$

In addition to the quantities associated with the wave beams, namely their angle θ_0 to the vertical, their half-width c and the coordinates $(x_\pm, z_\pm)$ perpendicular to and along them, respectively, this expression involves also quantities associated with the critical segments joining, for each beam, the opposite critical points on either side of the ellipse, namely their angle

$$\chi_0 = \arctan\left(\frac{b^2}{a^2}\tan\theta_0\right) \tag{4.32}$$

to the horizontal, their half-length

$$d = \frac{(a^4\cos^2\theta_0 + b^4\sin^2\theta_0)^{1/2}}{c}, \tag{4.33}$$

and the coordinates

$$\xi_\pm = x\cos\chi_0 \mp z\sin\chi_0, \quad \zeta_\pm = \pm x\sin\chi_0 + z\cos\chi_0 \tag{4.34a,b}$$

along and perpendicular to them, respectively. These quantities, introduced by Voisin (2020), are represented in figure 2.

We may then write

$$\xi \pm \mathrm{i}\eta = \operatorname{arccosh}\frac{x_\pm}{c} = \ln\left[\frac{x_\pm}{c} + \left(\frac{x_\pm^2}{c^2} - 1\right)^{1/2}\right], \tag{4.35}$$

on the understanding that the determination of the square roots is set by the replacement

$$x_\pm \to x_\pm \pm \mathrm{i}0\,\operatorname{sign}\zeta_\pm, \tag{4.36}$$

so that, in particular,

$$(x_\pm^2 - c^2)^{1/2} = |x_\pm^2 - c^2|^{1/2}\operatorname{sign} x_\pm \quad (|x_\pm| > c), \tag{4.37a}$$

$$= \pm\mathrm{i}|x_\pm^2 - c^2|^{1/2}\operatorname{sign}\zeta_\pm \quad (|x_\pm| < c). \tag{4.37b}$$

This determination, shown in figure 3, coincides with those in figures 3–4 of Hurley (1972) for a circular cylinder and figure 3 of Hurley (1997) for an elliptic cylinder.

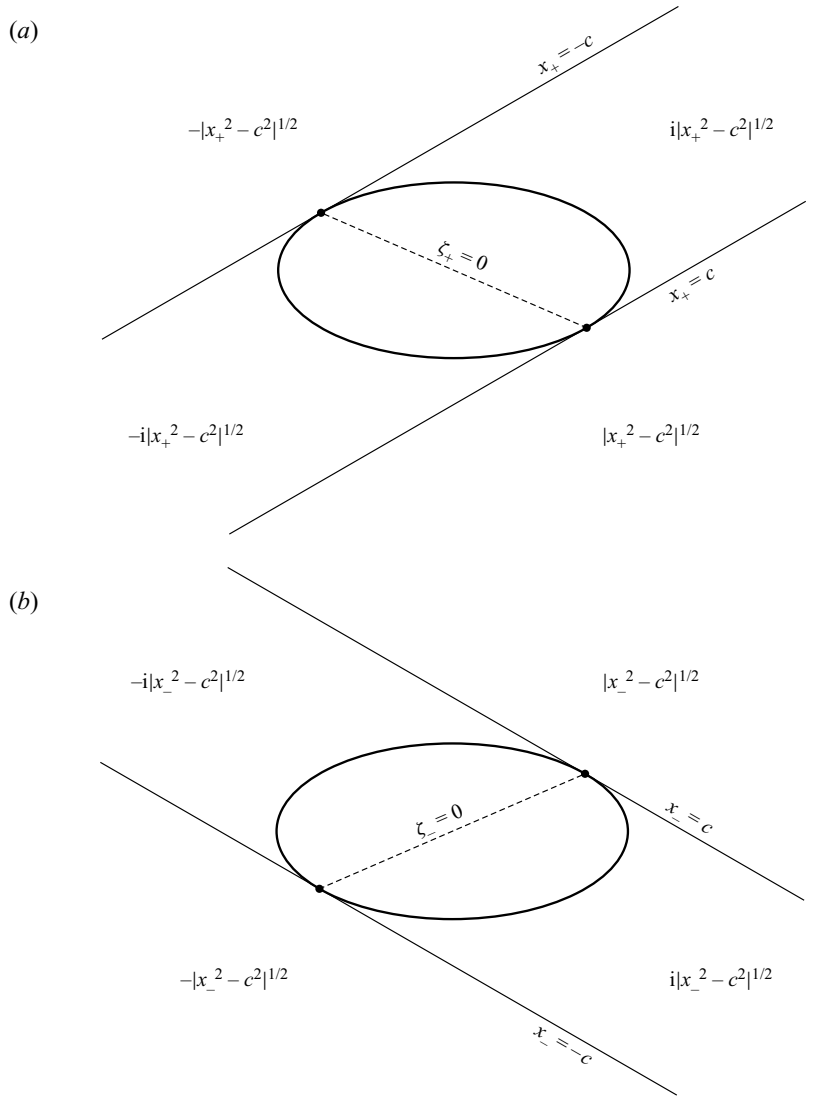

Figure 3. (*a*) Determinations of $(x_+^2 - c^2)^{1/2}$ and (*b*) determinations of $(x_-^2 - c^2)^{1/2}$.

It thus follows that

$$\xi = \frac{1}{2}\ln\left[\frac{x_-}{c} + \left(\frac{x_-^2}{c^2} - 1\right)^{1/2}\right] + \frac{1}{2}\ln\left[\frac{x_+}{c} + \left(\frac{x_+^2}{c^2} - 1\right)^{1/2}\right], \tag{4.38}$$

$$\eta = \frac{\mathrm{i}}{2}\ln\left[\frac{x_-}{c} + \left(\frac{x_-^2}{c^2} - 1\right)^{1/2}\right] - \frac{\mathrm{i}}{2}\ln\left[\frac{x_+}{c} + \left(\frac{x_+^2}{c^2} - 1\right)^{1/2}\right], \tag{4.39}$$

leading for the pressure to the expansion

$$p = \frac{1}{2}\rho_0 Nc \sin\theta_0 \sum_{\pm} \left\{ U_0^{(\mathrm{c})} \ln\left[\frac{x_\pm}{c} - \left(\frac{x_\pm^2}{c^2} - 1 \right)^{1/2} \right] + \sum_{m=1}^{\infty} \frac{\exp(\mathrm{i}m\eta_0)}{m} \left[U_m^{(\mathrm{c})} \pm \mathrm{i} U_m^{(\mathrm{s})} \right] \left[\frac{x_\pm}{c} - \left(\frac{x_\pm^2}{c^2} - 1 \right)^{1/2} \right]^m \right\}, \tag{4.40}$$

and for the velocity to

$$\boldsymbol{u} = -\frac{1}{2} \sum_{\pm} \frac{\boldsymbol{e}_{z_\pm}}{(x_\pm^2/c^2 - 1)^{1/2}} \sum_{m=0}^{\infty} \exp(\mathrm{i}m\eta_0) \left[(U_m^{(\mathrm{s})} \mp \mathrm{i} U_m^{(\mathrm{c})} \right] \left[\frac{x_\pm}{c} - \left(\frac{x_\pm^2}{c^2} - 1 \right)^{1/2} \right]^m, \tag{4.41}$$

with $\boldsymbol{e}_{z_\pm} = \pm \boldsymbol{e}_x \sin\theta_0 + \boldsymbol{e}_z \cos\theta_0$ a unit vector along the $z_\pm$-axis. Both expansions are of the form anticipated by Barcilon & Bleistein (1969) and Hurley (1972) for a circular cylinder.

At the ellipse (of contour C with outer side C_+), the pressure becomes

$$p(\boldsymbol{x} \in C_+) = \rho_0 Nc \sin\theta_0 \left[-\mathrm{i} U_0^{(\mathrm{c})} \eta_0 + \sum_{m=1}^{\infty} \frac{U_m^{(\mathrm{c})} \cos(m\eta) + U_m^{(\mathrm{s})} \sin(m\eta)}{m} \right], \tag{4.42}$$

and the velocity becomes

$$\boldsymbol{u}(\boldsymbol{x} \in C_+) = \frac{1}{2} \left\{ \left[\frac{\boldsymbol{e}_{z_+}}{\sin(\eta + \eta_0)} + \frac{\boldsymbol{e}_{z_-}}{\sin(\eta - \eta_0)} \right] \sum_{m=0}^{\infty} [U_m^{(\mathrm{c})} \cos(m\eta) + U_m^{(\mathrm{s})} \sin(m\eta)] + \mathrm{i} \left[\frac{\boldsymbol{e}_{z_+}}{\sin(\eta + \eta_0)} - \frac{\boldsymbol{e}_{z_-}}{\sin(\eta - \eta_0)} \right] \sum_{m=0}^{\infty} [U_m^{(\mathrm{s})} \cos(m\eta) - U_m^{(\mathrm{c})} \sin(m\eta)] \right\}. \tag{4.43}$$

Both the pressure and the normal velocity are regular, the latter being equal to its prescribed value U_n. The tangential velocity is singular at the critical points $\eta = \eta_0$, $\pi - \eta_0$, $\pi + \eta_0$ and $2\pi - \eta_0$; there, even at vanishingly small viscosity, the actual no-slip boundary condition will come into play, giving rise to the boundary-layer eruption predicted by Kerswell (1995) and Le Dizès & Le Bars (2017).

4.4. *Particular cases*

We consider now, as is usually done in acoustics, the simplest types of oscillations, associated with the lowest values of m; see Lighthill (1978, § 1.11) or Pierce (2019, §§ 4.1–2).

Monopolar oscillations, for which $m = 0$, correspond to radial pulsations at the velocity $\boldsymbol{U} = U\boldsymbol{x}/c$, such that

$$U_0^{(\mathrm{c})} = U\frac{ab}{c^2}, \quad U_0^{(\mathrm{s})} = 0. \tag{4.44a,b}$$

The associated pressure is uniform at the cylinder, with value

$$p(\boldsymbol{x} \in C_+) = -\mathrm{i}\rho_0 NU\frac{ab}{c}\sin\theta_0 \arctan\left(\frac{b}{a}\tan\theta_0\right). \tag{4.45}$$

This mode of oscillation, which in the presence of viscosity gives the lowest rate of decrease of the wave amplitude with distance away from the cylinder, is the least studied in the laboratory, having only been considered by Makarov, Neklyudov & Chashechkin (1990) and Machicoane *et al.* (2015) for a circular cylinder.

Dipolar oscillations, for which $m = 1$, correspond to back-and-forth vibrations of a rigid cylinder at the velocity $\boldsymbol{U} = U\boldsymbol{e}_x + W\boldsymbol{e}_z$, such that

$$U_1^{(\mathrm{c})} = U\frac{b}{c}, \quad U_1^{(\mathrm{s})} = W\frac{a}{c}. \tag{4.46a,b}$$

The pressure varies linearly with the Cartesian coordinates at the cylinder, in the form

$$p(\boldsymbol{x} \in C_+) = \rho_0 N\sin\theta_0\left(\frac{b}{a}Ux + \frac{a}{b}Wz\right). \tag{4.47}$$

This configuration is the most studied in the laboratory, from the visualizations of Mowbray & Rarity (1967) up to the quantitative measurements of Sutherland *et al.* (1999) and Zhang, King & Swinney (2007) for a circular cylinder and Sutherland & Linden (2002) for elliptic cylinders of aspect ratios $a/b = 1$, 2 and 3.

The expressions of the pressure and velocity at propagating frequencies $0 < \omega < N$ are given in table 3. For the vibrating cylinder they involve the notation

$$\alpha_\pm = \frac{\exp(\mathrm{i}\eta_0)}{2}\left(W\frac{a}{c} \mp \mathrm{i}U\frac{b}{c}\right) = \frac{(a\cos\theta_0 + \mathrm{i}b\sin\theta_0)(aW \mp \mathrm{i}bU)}{2c^2}, \tag{4.48}$$

introduced by Hurley (1997). They are accompanied by the limits $a \to 0$, corresponding to the horizontal vibrations of a vertical knife edge, considered theoretically by Llewellyn Smith & Young (2003) and experimentally by Peacock, Echeverri & Balmforth (2008), and $b \to 0$, corresponding to the vertical vibrations of a horizontal knife edge.

5. Spheroid

We move on to a spheroid of horizontal semi-axis a, vertical semi-axis b and equation

$$\frac{x^2}{a^2} + \frac{y^2}{a^2} + \frac{z^2}{b^2} = 1. \tag{5.1}$$

The approach remains the same as for the elliptic cylinder, but the exposition is made more intricate by the switch from hyperbolic functions to Legendre functions, and from circular functions to spherical harmonics. The relevant properties of these functions are recalled in Appendices A and B; they will be used silently in the following.

Pulsating cylinder	$p = \rho_0 NU \dfrac{ab}{2c} \sin\theta_0 \left\{ \ln\left[\dfrac{x_+}{c} - \left(\dfrac{x_+^2}{c^2} - 1 \right)^{1/2} \right] + \ln\left[\dfrac{x_-}{c} - \left(\dfrac{x_-^2}{c^2} - 1 \right)^{1/2} \right] \right\}$
	$\boldsymbol{u} = \mathrm{i} U \dfrac{ab}{2c} \left[\dfrac{\boldsymbol{e}_{z_+}}{(x_+^2 - c^2)^{1/2}} - \dfrac{\boldsymbol{e}_{z_-}}{(x_-^2 - c^2)^{1/2}} \right]$
Vibrating cylinder	$p = \mathrm{i}\rho_0 N \sin\theta_0 \{ \alpha_+ [x_+ - (x_+^2 - c^2)^{1/2}] - \alpha_- [x_- - (x_-^2 - c^2)^{1/2}] \}$
	$\boldsymbol{u} = \alpha_+ \boldsymbol{e}_{z_+} \left[1 - \dfrac{x_+}{(x_+^2 - c^2)^{1/2}} \right] + \alpha_- \boldsymbol{e}_{z_-} \left[1 - \dfrac{x_-}{(x_-^2 - c^2)^{1/2}} \right]$
Vertical knife edge	$p = \dfrac{\mathrm{i}}{2} \rho_0 NU [x_+ - (x_+^2 - b^2 \sin^2\theta_0)^{1/2} + x_- - (x_-^2 - b^2 \sin^2\theta_0)^{1/2}]$
	$\boldsymbol{u} = \dfrac{U}{2\sin\theta_0} \left\{ \boldsymbol{e}_{z_+} \left[1 - \dfrac{x_+}{(x_+^2 - b^2 \sin^2\theta_0)^{1/2}} \right] - \boldsymbol{e}_{z_-} \left[1 - \dfrac{x_-}{(x_-^2 - b^2 \sin^2\theta_0)^{1/2}} \right] \right\}$
Horizontal knife edge	$p = \dfrac{\mathrm{i}}{2} \rho_0 NW \tan\theta_0 [x_+ - (x_+^2 - a^2 \cos^2\theta_0)^{1/2} - x_- + (x_-^2 - a^2 \cos^2\theta_0)^{1/2}]$
	$\boldsymbol{u} = \dfrac{W}{2\cos\theta_0} \left\{ \boldsymbol{e}_{z_+} \left[1 - \dfrac{x_+}{(x_+^2 - a^2 \cos^2\theta_0)^{1/2}} \right] + \boldsymbol{e}_{z_-} \left[1 - \dfrac{x_-}{(x_-^2 - a^2 \cos^2\theta_0)^{1/2}} \right] \right\}$

Table 3. Pressure and velocity in the propagating frequency range $0 < \omega < N$. The determination of the square roots is set according to (4.36), becoming $x_\pm \to x_\pm + \mathrm{i}\,\mathrm{sign}\,x$ and $x_\pm \to x_\pm \pm \mathrm{i}\,\mathrm{sign}\,z$ for vertical and horizontal knife edges, respectively.

5.1. *Solution for $\omega > N$ and $(a/b)^2 + (N/\omega)^2 > 1$*

For $(a/b)^2 + (N/\omega)^2 > 1$, the coordinate stretching (3.17) transforms the original spheroid into an oblate one, of semi-axes $a_\star$ and $b_\star$ given by (4.2), and focal circle ($r_\star = c$, $z_\star = 0$). Here, $r_h = (x^2 + y^2)^{1/2}$ is the horizontal radial distance, stretched as $r_\star = (x_\star^2 + y_\star^2)^{1/2}$, and c is given by (4.3). We introduce oblate spheroidal coordinates (ξ, η, ϕ) defined by

$$r_\star = c \cosh\xi \sin\eta, \quad z_\star = c \sinh\xi \cos\eta, \tag{5.2a,b}$$

where $0 \leqslant \xi < \infty$ and $0 \leqslant \eta \leqslant \pi$, with $0 \leqslant \phi < 2\pi$ the usual azimuthal angle, such that

$$x_\star = r_\star \cos\phi, \quad y_\star = r_\star \sin\phi. \tag{5.3a,b}$$

In a given azimuthal plane, this definition is inverted in terms of the distances to the two foci in this plane,

$$r_\pm = [(r_\star \pm c)^2 + z_\star^2]^{1/2} = c(\cosh\xi \pm \sin\eta), \tag{5.4}$$

as

$$\cosh\xi = \frac{r_+ + r_-}{2c}, \quad \sin\eta = \frac{r_+ - r_-}{2c}; \tag{5.5a,b}$$

see Happel & Brenner (1983, Appendix A) or Landau & Lifshitz (1984, § 4). Differentiation is expressed as

$$c\frac{\partial}{\partial x_\star} = \frac{\cos\phi}{\sinh^2\xi+\cos^2\eta}\left(\sinh\xi\sin\eta\frac{\partial}{\partial\xi}+\cosh\xi\cos\eta\frac{\partial}{\partial\eta}\right)-\frac{\sin\phi}{\cosh\xi\sin\eta}\frac{\partial}{\partial\phi}, \quad (5.6a)$$

$$c\frac{\partial}{\partial y_\star} = \frac{\sin\phi}{\sinh^2\xi+\cos^2\eta}\left(\sinh\xi\sin\eta\frac{\partial}{\partial\xi}+\cosh\xi\cos\eta\frac{\partial}{\partial\eta}\right)+\frac{\cos\phi}{\cosh\xi\sin\eta}\frac{\partial}{\partial\phi}, \quad (5.6b)$$

$$c\frac{\partial}{\partial z_\star} = \frac{1}{\sinh^2\xi+\cos^2\eta}\left(\cosh\xi\cos\eta\frac{\partial}{\partial\xi}-\sinh\xi\sin\eta\frac{\partial}{\partial\eta}\right), \quad (5.6c)$$

where $\sinh^2\xi+\cos^2\eta=\cosh(\xi+\mathrm{i}\eta)\cosh(\xi-\mathrm{i}\eta)$.

At the spheroid, $\xi=\xi_0$ with ξ_0 given by (4.9), and

$$r_h = a\sin\eta, \quad z = b\cos\eta, \quad (5.7a,b)$$

implying that $\pi/2-\eta$ is Legendre's (1806) reduced latitude and Cayley's (1870) parametric latitude. The surface area element follows as

$$\mathrm{d}^2S = a(a^2\cos^2\eta+b^2\sin^2\eta)^{1/2}\,\mathrm{d}\Omega, \quad (5.8)$$

with $\mathrm{d}\Omega=\sin\eta\,\mathrm{d}\eta\,\mathrm{d}\phi$ the solid angle element, and the outward normal as

$$\boldsymbol{n} = \frac{b\boldsymbol{e}_{r_h}\sin\eta+a\boldsymbol{e}_z\cos\eta}{(a^2\cos^2\eta+b^2\sin^2\eta)^{1/2}}, \quad (5.9)$$

where $\boldsymbol{e}_{r_h}=\boldsymbol{e}_x\cos\phi+\boldsymbol{e}_y\sin\phi$ and $\boldsymbol{e}_\phi=-\boldsymbol{e}_x\sin\phi+\boldsymbol{e}_y\cos\phi$ are unit vectors along the radial and azimuthal horizontal directions, respectively, with $\boldsymbol{e}_y$ a unit vector along the y-axis. The boundary integral equation (3.5) becomes

$$4\pi\frac{N}{\omega}\Psi(\eta) = \int\left[\Psi(\eta',\phi')\frac{\partial}{\partial\xi'}+\frac{(a^2\cos^2\eta'+b^2\sin^2\eta')^{1/2}}{\omega(\omega^2-N^2)^{1/2}}U_n(\eta',\phi')\right]\frac{a\,\mathrm{d}\Omega'}{|\boldsymbol{x}_\star-\boldsymbol{x}'_\star|}, \quad (5.10)$$

where $\xi=\xi_0+0>\xi'=\xi_0$.

To solve it, we adapt the procedure used by Gorodtsov & Teodorovich (1982) for the potential flow around a sphere. The normal velocity $U_n(\eta,\phi)$ is expanded in spherical harmonics as

$$(a^2\cos^2\eta+b^2\sin^2\eta)^{1/2}U_n(\eta,\phi) = c\sum_{l=0}^{\infty}\sum_{m=-l}^{l}U_{lm}Y_l^m(\eta,\phi), \quad (5.11)$$

with

$$cU_{lm} = \int(a^2\cos^2\eta+b^2\sin^2\eta)^{1/2}U_n(\eta,\phi)\overline{Y_l^m(\eta,\phi)}\,\mathrm{d}\Omega, \quad (5.12)$$

where an overbar denotes a complex conjugate, and the surface potential $\Psi(\eta,\phi)$ as

$$\Psi(\eta,\phi) = \sum_{l=0}^{\infty}\sum_{m=-l}^{l}\Psi_{lm}Y_l^m(\eta,\phi), \quad (5.13)$$

with

$$\Psi_{lm} = \int\Psi(\eta,\phi)\overline{Y_l^m(\eta,\phi)}\,\mathrm{d}\Omega. \quad (5.14)$$

The expansion of the Green's function has been given by Morse & Feshbach (1953, p. 1296) and Hobson (1931, § 251), in both cases with typos: an extraneous factor 2 for the

former, and a missing factor i for the latter. Accordingly, the expansion has been rederived by an adaptation of the procedure of Jackson (1999, § 3.9), to get

$$\frac{c}{|\boldsymbol{x}_\star - \boldsymbol{x}'_\star|} = 4\mathrm{i}\pi \sum_{l=0}^{\infty} \sum_{m=-l}^{l} (-1)^m \frac{(l-m)!}{(l+m)!} P_l^m(\mathrm{i}\sinh\xi_<) Q_l^m(\mathrm{i}\sinh\xi_>) Y_l^m(\eta,\phi) \overline{Y_l^m(\eta',\phi')}, \tag{5.15}$$

where $\xi_< = \min(\xi, \xi')$ and $\xi_> = \max(\xi, \xi')$. The solution of (5.10) is then straightforward, in the form

$$\Psi_{lm} = -\frac{c}{\omega(\omega^2 - N^2)^{1/2}} \frac{U_{lm} Q_l^m(\mathrm{i}\sinh\xi_0)}{Q_l^{m+1}(\mathrm{i}\sinh\xi_0) + m\tanh\xi_0 Q_l^m(\mathrm{i}\sinh\xi_0)}. \tag{5.16}$$

Convolution according to (3.6), followed by differentiation according to (2.4), yields

$$p = \mathrm{i}\rho_0 c(\omega^2 - N^2)^{1/2} \sum_{l=0}^{\infty} \sum_{m=-l}^{l} \frac{U_{lm} Q_l^m(\mathrm{i}\sinh\xi) Y_l^m(\eta,\phi)}{Q_l^{m+1}(\mathrm{i}\sinh\xi_0) + m\tanh\xi_0 Q_l^m(\mathrm{i}\sinh\xi_0)} \tag{5.17}$$

for the pressure, and

$$\boldsymbol{u} = \sum_{l=0}^{\infty} \sum_{m=-l}^{l} \frac{U_{lm} Q_l^m(\mathrm{i}\sinh\xi) Y_l^m(\eta,\phi)}{Q_l^{m+1}(\mathrm{i}\sinh\xi_0) + m\tanh\xi_0 Q_l^m(\mathrm{i}\sinh\xi_0)} \left\{ m\left(1 - \frac{N^2}{\omega^2}\right)^{1/2} \frac{\boldsymbol{e}_{r_h} + \mathrm{i}\boldsymbol{e}_\phi}{\cosh\xi\,\sin\eta} \right.$$
$$\left. + \frac{1}{2} \sum_{\pm} \frac{(\omega^2 - N^2)^{1/2} \boldsymbol{e}_{r_h} \mp \mathrm{i}\omega \boldsymbol{e}_z}{N\cosh(\xi \pm \mathrm{i}\eta)} \left[\frac{\mathrm{P}_l^{m+1}(\cos\eta)}{\mathrm{P}_l^m(\cos\eta)} \pm \mathrm{i} \frac{Q_l^{m+1}(\mathrm{i}\sinh\xi)}{Q_l^m(\mathrm{i}\sinh\xi)} \right] \right\} \tag{5.18}$$

for the velocity.

5.2. *Solution for $\omega > N$ and $(a/b)^2 + (N/\omega)^2 < 1$*

For $(a/b)^2 + (N/\omega)^2 < 1$, we proceed as in § 4.2. The stretched spheroid becomes prolate, having foci at $(r_\star = 0, z_\star = \pm c')$, with c' given by (4.22). This leads to the introduction of prolate spheroidal coordinates (ξ', η, ϕ) defined by

$$r_\star = c' \sinh\xi' \sin\eta, \quad z_\star = c' \cosh\xi' \cos\eta, \tag{5.19a,b}$$

with $0 \leqslant \xi' < \infty$ and $0 \leqslant \eta \leqslant \pi$, so that

$$r_\star = c\cosh\left(\xi + \mathrm{i}\frac{\pi}{2}\right)\sin\eta, \quad z_\star = c\sinh\left(\xi + \mathrm{i}\frac{\pi}{2}\right)\cos\eta. \tag{5.20a,b}$$

Accordingly, the waves follow from those in § 5.1, by replacing ξ by $\xi' + \mathrm{i}\pi/2$ and c by $-\mathrm{i}c'$ throughout.

5.3. *Solution for $\omega < N$*

For $0 < \omega < N$, the waves propagate in beams inclined at the angle $\theta_0 = \arccos(\omega/N)$ to the vertical. The beams have half-width c given by (4.25), and are delimited by the critical rays tangential to the spheroid above and below, forming two double cones grazing the spheroid at critical circles of reduced latitude η_0 given by (4.27). The spheroid becomes

the surface $\xi = \mathrm{i}\eta_0$, and the waves are deduced by applying the transformation (3.18) to (5.17)–(5.18), writing $\xi_0 \to \mathrm{i}\eta_0 + 0$ so that

$$P_l^m(\mathrm{i}\sinh\xi_0) \to P_l^m(-\sin\eta_0 + \mathrm{i}0) = (-1)^l \mathrm{i}^m \,\mathrm{P}_l^m(\sin\eta_0), \tag{5.21}$$

$$Q_l^m(\mathrm{i}\sinh\xi_0) \to Q_l^m(-\sin\eta_0 + \mathrm{i}0) = (-1)^{l+1}\mathrm{i}^m \left(\mathrm{Q}_l^m + \mathrm{i}\frac{\pi}{2}\,\mathrm{P}_l^m\right)(\sin\eta_0). \tag{5.22}$$

For the complex coordinates ξ and η we proceed as in § 4.3, writing

$$\cosh\xi\sin\eta \sim \frac{r_h}{c}\left(\cos\theta_0 + \mathrm{i}\frac{\epsilon}{N}\frac{b^2}{c^2}\right), \quad \sinh\xi\cos\eta \sim \mathrm{i}\frac{z}{c}\left(\sin\theta_0 - \mathrm{i}\frac{\epsilon}{N}\frac{a^2}{c^2}\cot\theta_0\right), \tag{5.23a,b}$$

and thence

$$\sin(\eta \pm \mathrm{i}\xi) \sim \frac{x_\pm}{c} \pm \mathrm{i}\frac{\epsilon}{N}\frac{\zeta_\pm}{c}\frac{d}{c\sin\theta_0}, \tag{5.24}$$

where

$$x_\pm = r_h\cos\theta_0 \mp z\sin\theta_0, \quad z_\pm = \pm r_h\sin\theta_0 + z\cos\theta_0 \tag{5.25a,b}$$

are the characteristic coordinates associated with the wave beams, and

$$\xi_\pm = r_h\cos\chi_0 \mp z\sin\chi_0, \quad \zeta_\pm = \pm r_h\sin\chi_0 + z\cos\chi_0 \tag{5.26a,b}$$

are the coordinates associated with the truncated double cone joining the two critical circles at the surface of the spheroid. Here, χ_0, given by (4.32), is the angle of the generatrices of the double cone to the horizontal (in other words, the critical latitude), and d, given by (4.33), their half-length.

We then write

$$\xi \pm \mathrm{i}\left(\frac{\pi}{2} - \eta\right) = \operatorname{arccosh}\frac{x_\pm}{c} = 2\ln\left[\left(\frac{x_\pm + c}{2c}\right)^{1/2} + \left(\frac{x_\pm - c}{2c}\right)^{1/2}\right], \tag{5.27}$$

where the determination of the square roots is set by the replacement (4.36), yielding the combinations

$$\cosh\xi = \frac{1}{2}\left[\left(\frac{x_+}{c}+1\right)^{1/2}\left(\frac{x_-}{c}+1\right)^{1/2} + \left(\frac{x_+}{c}-1\right)^{1/2}\left(\frac{x_-}{c}-1\right)^{1/2}\right], \tag{5.28}$$

$$\sinh\xi = \frac{1}{2}\left[\left(\frac{x_+}{c}+1\right)^{1/2}\left(\frac{x_-}{c}-1\right)^{1/2} + \left(\frac{x_+}{c}-1\right)^{1/2}\left(\frac{x_-}{c}+1\right)^{1/2}\right], \tag{5.29}$$

$$\cos\eta = \frac{\mathrm{i}}{2}\left[\left(\frac{x_+}{c}+1\right)^{1/2}\left(\frac{x_-}{c}-1\right)^{1/2} - \left(\frac{x_+}{c}-1\right)^{1/2}\left(\frac{x_-}{c}+1\right)^{1/2}\right], \tag{5.30}$$

$$\sin\eta = \frac{1}{2}\left[\left(\frac{x_+}{c}+1\right)^{1/2}\left(\frac{x_-}{c}+1\right)^{1/2} - \left(\frac{x_+}{c}-1\right)^{1/2}\left(\frac{x_-}{c}-1\right)^{1/2}\right], \tag{5.31}$$

consistent with the determinations in § 4 of Davis (2012). The pressure is obtained as

$$p = -\mathrm{i}\rho_0 Nc\sin\theta_0 \times \sum_{l=0}^{\infty}\sum_{m=-l}^{l} \frac{(-1)^l(-i)^m U_{lm} Q_l^m(\mathrm{i}\sinh\xi) Y_l^m(\eta,\phi)}{\left(\mathrm{Q}_l^{m+1} + \mathrm{i}\frac{\pi}{2}\,\mathrm{P}_l^{m+1}\right)(\sin\eta_0) + m\tan\eta_0\left(\mathrm{Q}_l^m + \mathrm{i}\frac{\pi}{2}\,\mathrm{P}_l^m\right)(\sin\eta_0)}, \tag{5.32}$$

and the velocity as

$$\boldsymbol{u} = -\frac{\mathrm{i}}{2}\sum_{l=0}^{\infty}\sum_{m=-l}^{l}\frac{(-1)^l(-i)^m U_{lm} Q_l^m(\mathrm{i}\sinh\xi)Y_l^m(\eta,\phi)}{\left(\mathrm{Q}_l^{m+1}+\mathrm{i}\dfrac{\pi}{2}\mathrm{P}_l^{m+1}\right)(\sin\eta_0)+m\tan\eta_0\left(\mathrm{Q}_l^{m}+\mathrm{i}\dfrac{\pi}{2}\mathrm{P}_l^{m}\right)(\sin\eta_0)}$$
$$\times\sum_{\pm}\left\{m\frac{\boldsymbol{e}_\phi\sin\theta_0\mp\mathrm{i}\boldsymbol{e}_{z_\pm}}{\cosh\xi\sin\eta}+\frac{\boldsymbol{e}_{z_\pm}}{(x_\pm^2/c^2-1)^{1/2}}\left[\frac{\mathrm{P}_l^{m+1}(\cos\eta)}{\mathrm{P}_l^{m}(\cos\eta)}\mp\mathrm{i}\frac{Q_l^{m+1}(\mathrm{i}\sinh\xi)}{Q_l^{m}(\mathrm{i}\sinh\xi)}\right]\right\}, \tag{5.33}$$

where $\boldsymbol{e}_{z_\pm}=\pm\boldsymbol{e}_{r_h}\sin\theta_0+\boldsymbol{e}_z\cos\theta_0$ is a unit vector along the $z_\pm$-axis. The three-dimensional geometry breaks the relative simplicity of two-dimensional waves: the waves can no longer be separated into two components, one depending exclusively on x_+ and the other on x_-; instead, they are expressed in terms of the combinations (5.28)–(5.31), each of which involves both x_+ and x_-.

5.4. *Particular cases*

The simplest mode of oscillation of the spheroid is radial pulsations at the velocity $\boldsymbol{U}=U\boldsymbol{x}/c$. Such monopolar forcing is of degree $l=0$, with

$$U_{00}=\sqrt{4\pi}U\frac{ab}{c^2}. \tag{5.34}$$

The expressions of the pressure and velocity at propagating frequencies $0<\omega<N$ are given in table 4. They are consistent with Hendershott (1969), Appleby & Crighton (1987), Voisin (1991), Martin & Llewellyn Smith (2012) and Davis (2012) for a sphere. The pressure is uniform at the spheroid,

$$p(\boldsymbol{x}\in S_+)=\rho_0 NU\frac{a^2b}{c^2}\sin\theta_0\cos\theta_0\left[\frac{\pi}{2}-\mathrm{i}\,\mathrm{arcsinh}\left(\frac{b}{a}\tan\theta_0\right)\right], \tag{5.35}$$

as is expected for pulsations.

When the spheroid is rigid and vibrates back-and-forth with velocity $\boldsymbol{U}=U\boldsymbol{e}_x+V\boldsymbol{e}_y+W\boldsymbol{e}_z$, the forcing is dipolar and of degree $l=1$, with

$$U_{10}=\sqrt{\frac{4\pi}{3}}W\frac{a}{c},\quad U_{1,\pm1}=\sqrt{\frac{2\pi}{3}}(\mathrm{i}V\mp U)\frac{b}{c}. \tag{5.36a,b}$$

Introducing the ratio $\Upsilon=\tanh\xi_0$, that is

$$\Upsilon=\frac{b}{a}\left(1-\frac{N^2}{\omega^2}\right)^{1/2}\quad(\omega>N),\qquad \mathrm{i}\frac{b}{a}\tan\theta_0\quad(0<\omega<N), \tag{5.37a,b}$$

and the combination $D(\Upsilon)=\cosh^2\xi_0(1-\sinh\xi_0\,\mathrm{arccot}\sinh\xi_0)$, that is

$$D(\Upsilon)=\frac{1}{1-\Upsilon^2}\left[1-\frac{\Upsilon}{(1-\Upsilon^2)^{1/2}}\arccos\Upsilon\right]\quad(\omega>N\text{ and }\Upsilon<1), \tag{5.38a}$$
$$=\frac{1}{1-\Upsilon^2}\left[1-\frac{\Upsilon}{(\Upsilon^2-1)^{1/2}}\,\mathrm{arccosh}\,\Upsilon\right]\quad(\omega>N\text{ and }\Upsilon>1), \tag{5.38b}$$
$$=\frac{1}{1+|\Upsilon|^2}\left[1-\frac{|\Upsilon|}{(1+|\Upsilon|^2)^{1/2}}\left(\mathrm{i}\frac{\pi}{2}+\mathrm{arcsinh}\,|\Upsilon|\right)\right]\quad(0<\omega<N), \tag{5.38c}$$

the pressure and velocity become as given in table 4 for $0<\omega<N$. They are consistent with Sarma & Krishna (1972) and Lai & Lee (1981) for a spheroid, and Appleby

Pulsating spheroid	$p = \rho_0 NU \dfrac{a^2 b}{c^2} \sin\theta_0 \cos\theta_0 \operatorname{arccot}\sinh\xi$
	$\boldsymbol{u} = \mathrm{i}U \dfrac{a^2 b}{2c^2} \dfrac{\cos\theta_0}{\cosh\xi} \left[\dfrac{\boldsymbol{e}_{z_+}}{(x_+^2 - c^2)^{1/2}} - \dfrac{\boldsymbol{e}_{z_-}}{(x_-^2 - c^2)^{1/2}} \right]$
Vibrating spheroid	$p = \rho_0 N \dfrac{a^2 b}{c^2} \sin\theta_0 \cos\theta_0 \left[\dfrac{U\cos\phi + V\sin\phi}{1 + D(\Upsilon)} \cos\theta_0 (\cosh\xi \operatorname{arccot}\sinh\xi - \tanh\xi) \sin\eta \right.$
	$\left. - \mathrm{i} \dfrac{W}{1 - D(\Upsilon)} \sin\theta_0 (\sinh\xi \operatorname{arccot}\sinh\xi - 1) \cos\eta \right]$
	$\boldsymbol{u} = \mathrm{i} \dfrac{a^2 b}{c^3} \cos\theta_0 \left\{ \dfrac{U\sin\phi - V\cos\phi}{1 + D(\Upsilon)} \boldsymbol{e}_\phi \sin\theta_0 \cos\theta_0 \left(\operatorname{arccot}\sinh\xi - \dfrac{\sinh\xi}{\cosh^2\xi} \right) \right.$
	$+ \dfrac{1}{2} \sum_{\pm} \mp \dfrac{U\cos\phi + V\sin\phi}{1 + D(\Upsilon)} \boldsymbol{e}_{z_\pm} \cos\theta_0 \left[\operatorname{arccot}\sinh\xi - \dfrac{1}{\cosh^2\xi} \dfrac{x_\pm \cosh\xi + c\sin\eta}{(x_\pm^2 - c^2)^{1/2}} \right]$
	$\left. + \dfrac{1}{2} \sum_{\pm} \dfrac{W}{1 - D(\Upsilon)} \boldsymbol{e}_{z_\pm} \sin\theta_0 \left[\operatorname{arccot}\sinh\xi - \dfrac{1}{\cosh\xi} \dfrac{x_\pm}{(x_\pm^2 - c^2)^{1/2}} \right] \right\}$
	$D(\Upsilon) = \dfrac{a^2}{c^2} \cos^2\theta_0 \left\{ 1 - \dfrac{b}{c} \sin\theta_0 \left[\mathrm{i}\dfrac{\pi}{2} + \operatorname{arcsinh}\left(\dfrac{b}{a} \tan\theta_0 \right) \right] \right\}$
Horizontal circular disc	$p = -\dfrac{2}{\pi} \rho_0 NaW \sin\theta_0 (\sinh\xi \operatorname{arccot}\sinh\xi - 1) \cos\eta$
	$\boldsymbol{u} = \dfrac{W}{\pi\cos\theta_0} \sum_{\pm} \boldsymbol{e}_{z_\pm} \left[\operatorname{arccot}\sinh\xi - \dfrac{1}{\cosh\xi} \dfrac{x_\pm}{(x_\pm^2 - a^2\cos^2\theta_0)^{1/2}} \right]$

Table 4. Pressure and velocity in the propagating frequency range $0 < \omega < N$. The determination of the square roots is set according to (4.36), becoming $x_\pm \to x_\pm \pm \mathrm{i}\,\mathrm{sign}\, z$ for the horizontal disc.

& Crighton (1987), Martin & Llewellyn Smith (2012) and Davis (2012) for a sphere. Their relation to the experiments of Flynn, Onu & Sutherland (2003), King, Zhang & Swinney (2009), Voisin *et al.* (2011) and Ghaemsaidi & Peacock (2013) for a sphere will be discussed in § 6.2. At the spheroid, the pressure exhibits linear variations with the Cartesian coordinates,

$$p(\boldsymbol{x} \in S_+) = -\mathrm{i}\rho_0 N \sin\theta_0 \left[\frac{1 - D(\Upsilon)}{1 + D(\Upsilon)} (Ux + Vy) \cot\theta_0 - \frac{D(\Upsilon)}{1 - D(\Upsilon)} Wz \tan\theta_0 \right]. \quad (5.39)$$

The limit $a \to 0$ of the vibrating spheroid corresponds to a vertical needle, which generates no waves, and the limit $b \to 0$ to the heaving oscillations of a horizontal circular disc, considered theoretically by Sarma & Krishna (1972), Martin & Llewellyn Smith (2011) and Davis (2012) in an inviscid fluid and Davis & Llewellyn Smith (2010) in a viscous fluid, and experimentally by Bardakov, Vasil'ev & Chashechkin (2007). For the disc, we have

$$D(\Upsilon) \sim 1 - \frac{\pi}{2} \frac{b}{a} \left(1 - \frac{N^2}{\omega^2} \right)^{1/2}, \quad (5.40)$$

yielding the pressure and velocity in table 4.

6. Indirect approach

6.1. *Layer potentials*

Investigations so far have been based on the Kirchhoff–Helmholtz integral (3.4), combining the single-layer potential (3.7) and the double-layer potential (3.10). All the quantities involved are physically meaningful, either internal potential (hence pressure) inside the fluid in V_+, or internal potential and normal velocity on the side S_+ of the surface S of the body in contact with the fluid. By contrast, the layer potentials are purely mathematical entities, defined not only in the fluid but also inside the oscillating body in V_-. For each potential, the associated source density involves values of the potential and its derivative on both sides of S, inner for S_- and outer for S_+.

Specifically, the single-layer potential satisfies the differential equation

$$(N^2\nabla_h^2 - \omega^2\nabla^2)\psi_s = \sigma\delta_S, \tag{6.1}$$

implying (Schwartz 1966, § II.2.3) continuity of the potential and discontinuity of its modified normal derivative at S, namely

$$\psi_s(\boldsymbol{x} \in S_+) = \psi_s(\boldsymbol{x} \in S_-), \tag{6.2a}$$

$$\left(N^2\frac{\partial}{\partial n_h} - \omega^2\frac{\partial}{\partial n}\right)\psi_s(\boldsymbol{x} \in S_+) - \left(N^2\frac{\partial}{\partial n_h} - \omega^2\frac{\partial}{\partial n}\right)\psi_s(\boldsymbol{x} \in S_-) = \sigma(\boldsymbol{x}). \tag{6.2b}$$

As a consequence, the monopole density

$$\sigma(\boldsymbol{x}) = [\boldsymbol{u}_s(\boldsymbol{x} \in S_+) - \boldsymbol{u}_s(\boldsymbol{x} \in S_-)] \cdot \boldsymbol{n} \tag{6.3}$$

is equal to the discontinuity of the normal velocity at S, going from S_- to S_+. Similarly, the double-layer potential satisfies

$$(N^2\nabla_h^2 - \omega^2\nabla^2)\psi_d = -\left(N^2\frac{\partial}{\partial n_h} - \omega^2\frac{\partial}{\partial n}\right)(\mu\delta_S), \tag{6.4}$$

implying its discontinuity and the continuity of its modified normal derivative at S, with

$$\psi_d(\boldsymbol{x} \in S_+) - \psi_d(\boldsymbol{x} \in S_-) = -\mu(\boldsymbol{x}), \tag{6.5a}$$

$$\left(N^2\frac{\partial}{\partial n_h} - \omega^2\frac{\partial}{\partial n}\right)\psi_d(\boldsymbol{x} \in S_+) = \left(N^2\frac{\partial}{\partial n_h} - \omega^2\frac{\partial}{\partial n}\right)\psi_d(\boldsymbol{x} \in S_-). \tag{6.5b}$$

As a consequence, the dipole density

$$\mu(\boldsymbol{x}) = -[\psi_d(\boldsymbol{x} \in S_+) - \psi_d(\boldsymbol{x} \in S_-)] \tag{6.6}$$

is opposite to the discontinuity of the internal potential at S, going from S_- to S_+.

By imagining the oscillating body to be filled with fluid, it is possible to give physical meaning to each layer potential and to consider representing the motion of the whole fluid by this potential alone, without the other. For this, we adapt the procedure described for the Laplace and Helmholtz equations by Lamb (1932, §§ 57, 58 and 290) and Copley (1968). The volume V_- of the body is replaced by fictitious stratified fluid, of the same buoyancy frequency N as the real fluid outside. Applying Green's theorem (3.2) inside V_-, we obtain

for the internal potential ψ_f the Kirchhoff–Helmholtz integral

$$\int_S \left[G(\boldsymbol{x}-\boldsymbol{x}') \left(N^2 \frac{\partial}{\partial n'_h} - \omega^2 \frac{\partial}{\partial n'} \right) \psi_f(\boldsymbol{x}') - \psi_f(\boldsymbol{x}') \left(N^2 \frac{\partial}{\partial n'_h} - \omega^2 \frac{\partial}{\partial n'} \right) G(\boldsymbol{x}-\boldsymbol{x}') \right] \mathrm{d}^2 S'$$

$$= 0 \quad (\boldsymbol{x} \in V_+), \tag{6.7a}$$

$$= -\psi_f(\boldsymbol{x}) \quad (\boldsymbol{x} \in V_-), \tag{6.7b}$$

which combined with (3.4) gives

$$\int_S \left[G(\boldsymbol{x}-\boldsymbol{x}') \left(N^2 \frac{\partial}{\partial n'_h} - \omega^2 \frac{\partial}{\partial n'} \right) (\psi - \psi_f)(\boldsymbol{x}') \right.$$

$$\left. -(\psi - \psi_f)(\boldsymbol{x}') \left(N^2 \frac{\partial}{\partial n'_h} - \omega^2 \frac{\partial}{\partial n'} \right) G(\boldsymbol{x}-\boldsymbol{x}') \right] \mathrm{d}^2 S' = \psi(\boldsymbol{x}) \quad (\boldsymbol{x} \in V_+), \tag{6.8a}$$

$$= \psi_f(\boldsymbol{x}) \quad (\boldsymbol{x} \in V_-). \tag{6.8b}$$

The imposition of the boundary condition $\psi_f = \psi$ at S yields a single-layer field of monopole density

$$\sigma(\boldsymbol{x}) = [\boldsymbol{u}(\boldsymbol{x} \in S_+) - \boldsymbol{u}_f(\boldsymbol{x} \in S_-)] \cdot \boldsymbol{n}, \tag{6.9}$$

and similarly the condition $\boldsymbol{u}_f \cdot \boldsymbol{n} = \boldsymbol{u} \cdot \boldsymbol{n}$ yields a double-layer field of dipole density

$$\mu(\boldsymbol{x}) = -[\psi(\boldsymbol{x} \in S_+) - \psi_f(\boldsymbol{x} \in S_-)]. \tag{6.10}$$

In both cases the wave field is described by ψ outside S and ψ_f inside it.

A calculation of the waves based on the Kirchhoff–Helmholtz integral (3.4) is called direct, and a calculation based on the single-layer potential (3.7) or double-layer potential (3.10) is called indirect. The legitimacy of direct approaches follows from the derivation of the Kirchhoff–Helmholtz integral in § 3.1, but the legitimacy of indirect approaches remains to be seen. Paraphrasing Lamb (1932, § 290), it would be wrong to assume that, as in the case of the ordinary potential, a function ψ_f necessarily exists which satisfies the wave equation (2.3) throughout the finite region V_-, and also fulfils the condition that ψ_f or its modified normal derivative shall assume arbitrarily prescribed values over the boundary S.

6.2. *Equivalent source*

We consider the single layer (3.7), associated with the equivalent source (3.8). The boundary condition (2.5) yields for this source the integro-differential equation

$$U_n(\boldsymbol{x}) = \left(N^2 \frac{\partial}{\partial n_h} - \omega^2 \frac{\partial}{\partial n} \right) \int_S \sigma(\boldsymbol{x}') G(\boldsymbol{x}-\boldsymbol{x}') \, \mathrm{d}^2 S', \tag{6.11}$$

to be satisfied for all $\boldsymbol{x} \in S_+$.

In two dimensions, for the elliptic cylinder of § 4, the equation becomes

$$2\pi U_n(\eta) = \frac{\partial}{\partial \xi} \int_0^{2\pi} \left(\frac{a^2 \sin^2 \eta' + b^2 \cos^2 \eta'}{a^2 \sin^2 \eta + b^2 \cos^2 \eta} \right)^{1/2} \sigma(\eta') \ln |\boldsymbol{x}_\star - \boldsymbol{x}'_\star| \, \mathrm{d}\eta', \tag{6.12}$$

where $\xi = \xi_0 + 0 > \xi' = \xi_0$. Expanding the source density $\sigma(\eta)$ as

$$(a^2 \sin^2 \eta + b^2 \cos^2 \eta)^{1/2} \sigma(\eta) = c \sum_{m=0}^{\infty} \left[\sigma_m^{(\mathrm{c})} \cos(m\eta) + \sigma_m^{(\mathrm{s})} \sin(m\eta) \right], \tag{6.13}$$

and the normal velocity $U_n(\eta)$ as (4.14), the solution is obtained immediately as

$$\sigma_m^{(\mathrm{c})} = [1 + \tanh(m\xi_0)] U_m^{(\mathrm{c})}, \quad \sigma_m^{(\mathrm{s})} = [1 + \coth(m\xi_0)] U_m^{(\mathrm{s})}. \tag{6.14a,b}$$

The waves (4.20)–(4.21) then follow from (3.7) and (2.4).

The cylinder is thus equivalent to the source

$$q(\boldsymbol{x}) = \frac{c}{ab} \delta \left[\left(\frac{x^2}{a^2} + \frac{z^2}{b^2} \right)^{1/2} - 1 \right] \sum_{m=0}^{\infty} [\sigma_m^{(\mathrm{c})} \cos(m\eta) + \sigma_m^{(\mathrm{s})} \sin(m\eta)], \tag{6.15}$$

of spectrum

$$q(\boldsymbol{k}) = 2\pi c \sum_{m=0}^{\infty} (-\mathrm{i})^m \, \mathrm{J}_m[(k_x^2 a^2 + k_z^2 b^2)^{1/2}] [\sigma_m^{(\mathrm{c})} \cos(m\eta_k) + \sigma_m^{(\mathrm{s})} \sin(m\eta_k)], \tag{6.16}$$

where J_m denotes a cylindrical Bessel function, $\boldsymbol{k} = (k_x, k_z)$ the wave vector and η_k the angle such that

$$k_x a = \left(k_x^2 a^2 + k_z^2 b^2 \right)^{1/2} \cos \eta_k, \quad k_z b = \left(k_x^2 a^2 + k_z^2 b^2 \right)^{1/2} \sin \eta_k. \tag{6.17a,b}$$

The knowledge of this spectrum provides an alternative expression of the waves, into which the effect of viscous attenuation can be added following Lighthill (1978, § 4.10) at large distance from the source, and Voisin (2020) at arbitrary distance from it.

We use the latter. In an inviscid fluid, the velocity outside a source of mass $q(x, z)$ of support the elliptic domain $x^2/a^2 + z^2/b^2 < 1$ is given in the propagating frequency range $0 < \omega < N$ by

$$\boldsymbol{u} = \frac{1}{4\pi} \sum_{\pm} \boldsymbol{e}_{z_\pm} \operatorname{sign} \zeta_\pm \int_0^\infty q_\pm(k_{x_\pm} = \pm\kappa \operatorname{sign} \zeta_\pm, k_{z_\pm} = 0) \exp(\pm \mathrm{i}\kappa x_\pm \operatorname{sign} \zeta_\pm) \, \mathrm{d}\kappa, \tag{6.18}$$

where

$$k_{x_\pm} = k_x \cos\theta_0 \mp k_z \sin\theta_0, \quad k_{z_\pm} = \pm k_x \sin\theta_0 + k_z \cos\theta_0, \tag{6.19a,b}$$

and $q_\pm(k_{x_\pm}, k_{z_\pm}) = q(k_x, k_z)$. For the cylinder, the spectrum (6.16) becomes

$$q_\pm(k_{x_\pm}, k_{z_\pm} = 0) = 2\pi c \sum_{m=0}^{\infty} (-\mathrm{i})^m \exp(\mathrm{i}m\eta_0) \left[U_m^{(\mathrm{c})} \pm \mathrm{i} U_m^{(\mathrm{s})} \right] \mathrm{J}_m(k_{x_\pm} c), \tag{6.20}$$

so that

$$\boldsymbol{u} = c\sum_{\pm}\boldsymbol{e}_{z_\pm}\sum_{m=0}^{\infty}(\mp\mathrm{i}\,\mathrm{sign}\,\zeta_\pm)^m\exp(\mathrm{i}m\eta_0)\left[U_m^{(\mathrm{c})}\pm\mathrm{i}U_m^{(\mathrm{s})}\right]$$
$$\times\int_0^\infty \mathrm{J}_m(\kappa c)\exp(\pm\mathrm{i}\kappa x_\pm\,\mathrm{sign}\,\zeta_\pm)\,\mathrm{d}\kappa. \tag{6.21}$$

Using the transform

$$\int_0^\infty \mathrm{J}_m(k)\exp(\mathrm{i}kx)\,\mathrm{d}k = \mathrm{i}^{m+1}\frac{\{x-[(x+\mathrm{i}0)^2-1]^{1/2}\}^m}{[(x+\mathrm{i}0)^2-1]^{1/2}}, \tag{6.22}$$

taken from table 5 of Voisin (2003), the velocity (4.41) is recovered. Viscosity, at large Stokes number $\omega c^2/\nu \gg 1$ with ν the kinematic viscosity, adds an exponential attenuation factor inside the integrand of (6.21), transforming it into

$$\boldsymbol{u} = c\sum_{\pm}\boldsymbol{e}_{z_\pm}\sum_{m=0}^{\infty}(\mp\mathrm{i}\,\mathrm{sign}\,\zeta_\pm)^m\exp(\mathrm{i}m\eta_0)\left[U_m^{(\mathrm{c})}\pm\mathrm{i}U_m^{(\mathrm{s})}\right]$$
$$\times\int_0^\infty \mathrm{J}_m(\kappa c)\exp\left(-\beta\kappa^3\frac{d}{c}|\zeta_\pm|\right)\exp(\pm\mathrm{i}\kappa x_\pm\,\mathrm{sign}\,\zeta_\pm)\,\mathrm{d}\kappa, \tag{6.23}$$

with $\beta = \nu/(2N\sin\theta_0)$.

In three dimensions, for the spheroid of § 5, the integro-differential equation (6.11) becomes

$$4\pi\frac{N}{\omega}U_n(\eta,\phi) = -\frac{\partial}{\partial\xi}\int\left(\frac{a^2\cos^2\eta'+b^2\sin^2\eta'}{a^2\cos^2\eta+b^2\sin^2\eta}\right)^{1/2}\sigma(\eta',\phi')\frac{a\,\mathrm{d}\Omega'}{|\boldsymbol{x}_\star-\boldsymbol{x}'_\star|}, \tag{6.24}$$

where $\xi = \xi_0 + 0 > \xi' = \xi_0$. Expanding $\sigma(\eta,\phi)$ as

$$(a^2\cos^2\eta+b^2\sin^2\eta)^{1/2}\sigma(\eta,\phi) = c\sum_{l=0}^{\infty}\sum_{m=-l}^{l}\sigma_{lm}Y_l^m(\eta,\phi), \tag{6.25}$$

and $U_n(\eta,\phi)$ as (5.11), we obtain

$$\sigma_{lm} = \mathrm{i}\frac{(l+m)!}{(l-m)!}\frac{(-1)^m}{P_l^m(\mathrm{i}\sinh\xi_0)}\frac{U_{lm}}{\cosh\xi_0 Q_l^{m+1}(\mathrm{i}\sinh\xi_0)+m\sinh\xi_0 Q_l^m(\mathrm{i}\sinh\xi_0)}, \tag{6.26}$$

which leads to the waves (5.17)–(5.18). The spheroid is thus represented by the source

$$q(\boldsymbol{x}) = \frac{c}{ab}\delta\left[\left(\frac{r_h^2}{a^2}+\frac{z^2}{b^2}\right)^{1/2}-1\right]\sum_{l=0}^{\infty}\sum_{m=-l}^{l}\sigma_{lm}Y_l^m(\eta,\phi). \tag{6.27}$$

Its spectrum is obtained using (A14) as

$$q(\boldsymbol{k}) = 4\pi ac\sum_{l=0}^{\infty}(-\mathrm{i})^l\,\mathrm{j}_l[(\kappa_h^2a^2+k_z^2b^2)^{1/2}]\sum_{m=-l}^{l}\sigma_{lm}Y_l^m(\eta_k,\phi_k), \tag{6.28}$$

where j_l denotes a spherical Bessel function, $\boldsymbol{k} = (k_x, k_y, k_z)$ the wave vector, of horizontal modulus $\kappa_h = (k_x^2 + k_y^2)^{1/2}$, and the angles (η_k, ϕ_k) are such that

$$\kappa_h a = \left(\kappa_h^2 a^2 + k_z^2 b^2\right)^{1/2} \sin\eta_k, \quad k_z b = \left(\kappa_h^2 a^2 + k_z^2 b^2\right)^{1/2} \cos\eta_k, \tag{6.29a,b}$$

and

$$k_x = \kappa_h \cos\phi_k, \quad k_y = \kappa_h \sin\phi_k, \tag{6.30a,b}$$

respectively.

The equivalent sources for the particular cases of §§ 4.4 and 5.4 are gathered in table 5. For line sources in two dimensions, obtained as the limit of an ellipse of zero thickness perpendicular to the line, and for plane sources in three dimensions, obtained as the limit of a spheroid of zero thickness perpendicular to the plane, the opposite single layers on either side of the line or plane collapse into a double layer as the thickness goes to zero.

For a vibrating circular cylinder, adding viscous attenuation according to (6.23), the same waves are obtained as in Hurley & Keady (1997), compared satisfactorily with experiment by Sutherland *et al.* (1999) and Zhang *et al.* (2007). For a vibrating elliptic cylinder and a vertical knife edge, the sources have been shown by Voisin (2020) to be consistent with the measurements of Sutherland & Linden (2002) and Peacock *et al.* (2008), respectively. For a vibrating sphere, the source has been used by Voisin *et al.* (2011) to propose an expression of the waves which compares successfully with the experiments of Flynn *et al.* (2003), King *et al.* (2009), Voisin *et al.* (2011) and Ghaemsaidi & Peacock (2013).

6.3. *Relation to the direct approach*

Now, the direct approach also leads to an equivalent source (3.13), of spectrum (3.15). Writing, for the elliptic cylinder,

$$\boldsymbol{n}\cdot(N^2 k_x \boldsymbol{e}_x - \omega^2 \boldsymbol{k}) = N^2 \frac{c^2}{ab}\left(\frac{k_x^2 a^2 + k_z^2 b^2}{a^2\sin^2\eta + b^2\cos^2\eta}\right)^{1/2} (\sinh^2\xi_0 \cos\eta\cos\eta_k + \cosh^2\xi_0 \sin\eta\sin\eta_k), \tag{6.31}$$

and using (4.19), we obtain, after some algebra,

$$\begin{aligned} q(\boldsymbol{k}) = {} & 2\pi c \sum_{m=0}^{\infty} (-\mathrm{i})^m \mathrm{J}_m[(k_x^2 a^2 + k_z^2 b^2)^{1/2}] \\ & \times \left\{ U_m^{(\mathrm{c})} \left[\cos(m\eta_k) - \frac{\sin\eta_k\cos\eta_k}{\sinh\xi_0\cosh\xi_0}\sin(m\eta_k)\right] \right. \\ & \left. + U_m^{(\mathrm{s})} \left[\sin(m\eta_k) + \frac{\sin\eta_k\cos\eta_k}{\sinh\xi_0\cosh\xi_0}\cos(m\eta_k)\right]\right\} \\ & + \pi c \frac{\sinh\xi_0^2 + \sin^2\eta_k}{\sinh\xi_0\cosh\xi_0}(k_x^2 a^2 + k_z^2 b^2)^{1/2} \left\{ 2\,\mathrm{J}_1[(k_x^2 a^2 + k_z^2 b^2)^{1/2}]\xi_0 U_0^{(\mathrm{c})} \right. \\ & \left. - \sum_{m=1}^{\infty} (\mathrm{J}_{m+1} - \mathrm{J}_{m-1})[(k_x^2 a^2 + k_z^2 b^2)^{1/2}] \frac{U_m^{(\mathrm{c})}\cos(m\eta_k) + U_m^{(\mathrm{s})}\sin(m\eta_k)}{m} \right\}, \end{aligned} \tag{6.32}$$

https://doi.org/10.1017/jfm.2021.729 Published online by Cambridge University Press

Oscillating body	$q(\boldsymbol{x})$	$q(\boldsymbol{k})$
Pulsating cylinder	$\dfrac{U}{c}\delta\left[\left(\dfrac{x^2}{a^2}+\dfrac{z^2}{b^2}\right)^{1/2}-1\right]$	$2\pi U\dfrac{ab}{c}\,\mathrm{J}_0[(k_x^2a^2+k_z^2b^2)^{1/2}]$
Vibrating cylinder	$\left[(1+\Upsilon)U\dfrac{x}{a^2}+\left(1+\dfrac{1}{\Upsilon}\right)W\dfrac{z}{b^2}\right]\delta\left[\left(\dfrac{x^2}{a^2}+\dfrac{z^2}{b^2}\right)^{1/2}-1\right]$	$-2\mathrm{i}\pi ab\left[(1+\Upsilon)Uk_x+\left(1+\dfrac{1}{\Upsilon}\right)Wk_z\right]\dfrac{\mathrm{J}_1[(k_x^2a^2+k_z^2b^2)^{1/2}]}{(k_x^2a^2+k_z^2b^2)^{1/2}}$
Vertical knife edge	$-2U\left(1-\dfrac{N^2}{\omega^2}\right)^{1/2}H(b-\lvert z\rvert)(b^2-z^2)^{1/2}\delta'(x)$	$-2\mathrm{i}\pi bU\left(1-\dfrac{N^2}{\omega^2}\right)^{1/2}\dfrac{k_x}{k_z}\,\mathrm{J}_1(k_zb)$
Horizontal knife edge	$-2W\left(1-\dfrac{N^2}{\omega^2}\right)^{-1/2}H(a-\lvert x\rvert)(a^2-x^2)^{1/2}\delta'(z)$	$-2\mathrm{i}\pi aW\left(1-\dfrac{N^2}{\omega^2}\right)^{-1/2}\dfrac{k_z}{k_x}\,\mathrm{J}_1(k_xa)$
Pulsating spheroid	$\dfrac{U}{c}\delta\left[\left(\dfrac{r_h^2}{a^2}+\dfrac{z^2}{b^2}\right)^{1/2}-1\right]$	$4\pi U\dfrac{a^2b}{c}\,\mathrm{j}_0[(\kappa_h^2a^2+k_z^2b^2)^{1/2}]$
Vibrating spheroid	$\left[\dfrac{2}{1+D(\Upsilon)}\left(U\dfrac{x}{a^2}+V\dfrac{y}{a^2}\right)+\dfrac{W}{1-D(\Upsilon)}\dfrac{z}{b^2}\right]\delta\left[\left(\dfrac{r_h^2}{a^2}+\dfrac{z^2}{b^2}\right)^{1/2}-1\right]$	$-4\mathrm{i}\pi a^2b\left[2\dfrac{Uk_x+Vk_y}{1+D(\Upsilon)}+\dfrac{Wk_z}{1-D(\Upsilon)}\right]\dfrac{\mathrm{j}_1[(\kappa_h^2a^2+k_z^2b^2)^{1/2}]}{(\kappa_h^2a^2+k_z^2b^2)^{1/2}}$
Horizontal circular disc	$-\dfrac{4}{\pi}W\left(1-\dfrac{N^2}{\omega^2}\right)^{-1/2}H(a-r_h)(a^2-r_h^2)^{1/2}\delta'(z)$	$-8\mathrm{i}a^2W\left(1-\dfrac{N^2}{\omega^2}\right)^{-1/2}\dfrac{k_z}{\kappa_h}\,\mathrm{j}_1(\kappa_ha)$

Table 5. Equivalent sources and associated spectra for the oscillating bodies considered in §§ 4.4 and 5.4, with Υ and $D(\Upsilon)$ defined in (5.37)–(5.38).

a result significantly more complicated than (6.16). The two spectra coincide at the wave vectors satisfying the dispersion relation $\omega^2(k_x^2 + k_z^2) = N^2 k_x^2$, that is $\sinh \xi_0^2 + \sin^2 \eta_k = 0$, namely $\eta_k = \pm \mathrm{i}\xi_0$, which alone contribute to wave radiation. Accordingly, the effect of the indirect approach is to filter out, in the spectrum of the oscillating body, the wave vectors that do not play a role in its wave radiation.

However, the direct approach is not always possible. This can be seen with the example of an inclined vibrating elliptic cylinder, of major axis making the angle ϕ_0 to the horizontal. The results of Hurley (1997), combined with the theory of Voisin (2020), imply a spectrum of the form given in table 5 for a cylinder of horizontal and vertical axes, but with the angle θ_0 replaced, in the definition (5.37*b*) of Υ, by $\theta_0 + \phi_0$ for the beams of waves propagating upward to the right and downward to the left, and $\theta_0 - \phi_0$ for the beams propagating downward to the right and upward to the left. Such different spectra for the different wave beams cannot be achieved with the indirect approach, and require the switch to the direct approach.

In a related way, Hurley & Keady (1997, Appendix B) considered the representation of the cylinder by line distributions of point vortices, and also obtained two different distributions, one per beam, where the vortices are distributed along the critical segment $\zeta_\pm = 0$ joining, for this beam, the critical points on either side of the cylinder; see figures 2 and 3.

The limitation of indirect approaches becomes more explicit for an inclined knife edge, making the angle ϕ_0 to the horizontal. Introducing inclined coordinates

$$x_0 = x\cos\phi_0 + z\sin\phi_0, \quad z_0 = -x\sin\phi_0 + z\cos\phi_0, \tag{6.33a,b}$$

the imposed normal velocity at the knife edge at $z_0 = 0$ induces a pressure discontinuity across it, $2p_0(x_0) = p(x_0, z_0 = +0) - p(x_0, z_0 = -0)$. Elementary manipulation of the equations of motion for $0 < \omega < N$ yields a velocity divergence, hence a source of mass,

$$q(\boldsymbol{x}) = 2\mathrm{i}\frac{p_0(x_0)\delta'(z_0)\cos(\theta_0 + \phi_0)\cos(\theta_0 - \phi_0) + p_0'(x_0)\delta(z_0)\sin\phi_0\cos\phi_0}{\rho_0 N \sin^2\theta_0\cos\theta_0}. \tag{6.34}$$

When the knife edge is either horizontal ($\phi_0 = 0$) or vertical ($\phi_0 = \pi/2$), a double layer is obtained, consistent with table 5. But when the knife edge is truly inclined, a combination of single and double layers is obtained.

Accordingly, the possibility of using an indirect representation of an oscillating body for generation problems is seen to require some degree of symmetry of the body with respect to the horizontal and the vertical. By contrast, Martin & Llewellyn Smith (2012) showed that a double layer suffices for scattering problems, irrespective of the shape of the scatterer.

7. Boundary values

The possibility of solving analytically the boundary integral equations for the cylinder and the spheroid has resulted from the availability of expansions (4.18) and (5.15) of the Green's function, allowing the limit to be taken in which $\boldsymbol{x}$ approaches S asymptotically. When the equations are considered numerically, a procedure is required for which $\boldsymbol{x}$ is exactly on S. Given the singularity of the Green's function at $\boldsymbol{x}' = \boldsymbol{x}$, this requires the evaluation of the surface integral as an improper one, in which a vicinity of $\boldsymbol{x}$ is excluded and the contribution of this vicinity is evaluated separately. Ordinarily, as a result, the Kirchhoff–Helmholtz integral evaluates to one half the value that would be obtained if $\boldsymbol{x}$ were just outside S; see, for example, Brebbia *et al.* (1984, chapter 2), Pozrikidis (1992, chapter 2; 2002, chapters 2 and 4) or Gaul *et al.* (2003, chapter 4).

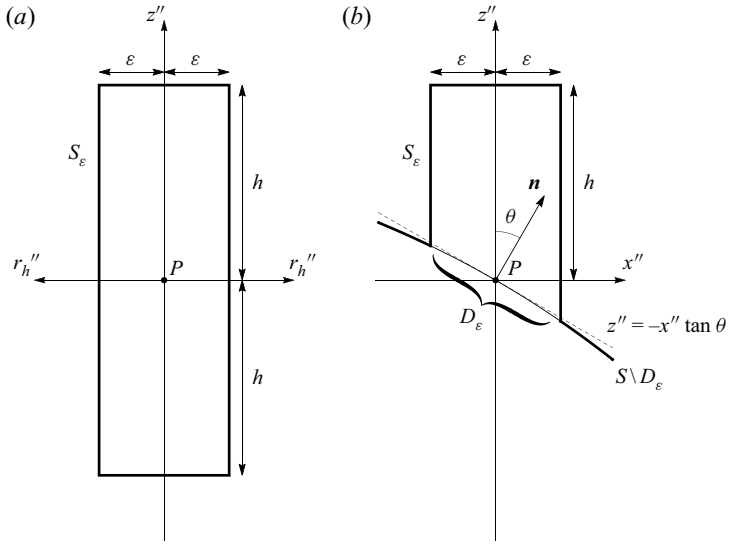

Figure 4. Small cylindrical surface S_ϵ around a point P situated either (a) outside or (b) at the surface S, for the calculation of the Kirchhoff–Helmholtz integral at P.

For monochromatic internal waves, Martin & Llewellyn Smith (2012) surrounded $\boldsymbol{x}$, as is usually done, by a small hemisphere. They obtained, not the usual factor $1/2$, but rather a complicated factor depending on the frequency and on the inclination of the normal to S at $\boldsymbol{x}$. This is at apparent odds with Gorodtsov & Teodorovich (1982), who gave the factor $1/2$ without justification for the internal waves emitted a body in uniform translation, and Kapitonov (1980), who obtained the same factor $1/2$ for unsteady inertial waves, based on earlier work by Sobolev (1954), replacing the hemisphere by a small vertical cylinder.

7.1. *Kirchhoff–Helmholtz integral*

We adapt here Sobolev's and Kapitonov's procedure to monochromatic internal waves, on the implicit assumption that $\omega > N$. For this, we revisit first the Kirchhoff–Helmholtz integral (3.4), derived in § 3.1 by distribution theory, applying classical function theory to the volume delimited by the surface S of the body, the surface S_∞ at infinity and, if $\boldsymbol{x}$ is situated outside the body, a circular cylinder S_ϵ of centre at $\boldsymbol{x}$, vertical axis, height $2h$ and horizontal radius $\epsilon \to 0$, shown in figure 4(a). For simplicity all lengths are assumed non-dimensional, based on some length scale of the forcing. Sobolev (1954) kept h finite, while Kapitonov (1980) set $h = \epsilon^{3/4}$; we keep h finite for now, and will see later how the necessity arises to set $h \to 0$ while preserving $\epsilon/h = o(1)$.

When $\boldsymbol{x}$ is situated inside S, the derivation is exactly the same as before, yielding (3.4b). When $\boldsymbol{x}$ is situated outside S, we write

$$\left(\int_{S_\epsilon} + \int_S\right)\left[G(\boldsymbol{x}-\boldsymbol{x}')\left(N^2\frac{\partial}{\partial n_h'} - \omega^2\frac{\partial}{\partial n'}\right)\psi(\boldsymbol{x}') - \psi(\boldsymbol{x}')\left(N^2\frac{\partial}{\partial n_h'} - \omega^2\frac{\partial}{\partial n'}\right)G(\boldsymbol{x}-\boldsymbol{x}')\right]\mathrm{d}^2S' = 0, \tag{7.1}$$

that is

$$\left(\int_{S_\epsilon}+\int_{S}\right)[\boldsymbol{u}(\boldsymbol{x}')\cdot\boldsymbol{n}'G(\boldsymbol{x}'-\boldsymbol{x})-\psi(\boldsymbol{x}')\boldsymbol{u}_G(\boldsymbol{x}'-\boldsymbol{x})\cdot\boldsymbol{n}']\,\mathrm{d}^2S'=0. \tag{7.2}$$

On S_ϵ we introduce cylindrical polar coordinates (r_h'', ϕ'', z'') for the position $\boldsymbol{x}''=\boldsymbol{x}'-\boldsymbol{x}$ relative to $\boldsymbol{x}$, as shown in figure 4(*a*). On the horizontal part $S_\epsilon^{(h)}$ of S_ϵ, we have

$$0<r_h''<\epsilon,\quad 0<\phi''<2\pi,\quad z''=\pm h,\quad \boldsymbol{n}'=\pm\boldsymbol{e}_{z''},\quad \mathrm{d}^2S'=r_h''\,\mathrm{d}r_h''\,\mathrm{d}\phi'', \tag{7.3a–e}$$

yielding

$$\int_{S_\epsilon^{(h)}}G(\boldsymbol{x}'')\,\mathrm{d}^2S'=\frac{h}{\omega^2}\left[\left(1+\frac{\omega^2}{\omega^2-N^2}\frac{\epsilon^2}{h^2}\right)^{1/2}-1\right]\sim\frac{\epsilon^2}{2(\omega^2-N^2)h}, \tag{7.4a}$$

$$\int_{S_\epsilon^{(h)}}\boldsymbol{u}_G(\boldsymbol{x}'')\cdot\boldsymbol{n}'\,\mathrm{d}^2S'=1-\left(1+\frac{\omega^2}{\omega^2-N^2}\frac{\epsilon^2}{h^2}\right)^{-1/2}\sim\frac{\omega^2\epsilon^2}{2(\omega^2-N^2)h^2}. \tag{7.4b}$$

With ψ and $u_{z''}$ bounded over $S_\epsilon^{(h)}$, the contribution of $S_\epsilon^{(h)}$ is seen to vanish as $\epsilon\to0$. On the vertical part $S_\epsilon^{(v)}$ of S_ϵ, we have

$$r_h''=\epsilon,\quad 0<\phi''<2\pi,\quad -h<z''<h,\quad \boldsymbol{n}'=\boldsymbol{e}_{r_h''},\quad \mathrm{d}^2S'=\epsilon\,\mathrm{d}\phi''\,\mathrm{d}z'', \tag{7.5a–e}$$

yielding

$$\int_{S_\epsilon^{(v)}}G(\boldsymbol{x}'')\,\mathrm{d}^2S'=\frac{\epsilon}{\omega^2-N^2}\operatorname{arcsinh}\left[\frac{(\omega^2-N^2)^{1/2}}{\omega}\frac{h}{\epsilon}\right]\sim\frac{\epsilon}{\omega^2-N^2}\ln\frac{h}{\epsilon}, \tag{7.6a}$$

$$\int_{S_\epsilon^{(v)}}\boldsymbol{u}_G(\boldsymbol{x}'')\cdot\boldsymbol{n}'\,\mathrm{d}^2S'=\left(1+\frac{\omega^2}{\omega^2-N^2}\frac{\epsilon^2}{h^2}\right)^{-1/2}\sim1-\frac{\omega^2\epsilon^2}{2(\omega^2-N^2)h^2}. \tag{7.6b}$$

An additional assumption $h\to0$ is required, so that not only ψ and $u_{r_h''}$ are bounded on $S_\epsilon^{(v)}$, but also $\psi(\boldsymbol{x}')$ may be made as close to $\psi(\boldsymbol{x})$ as desired, while ensuring $\epsilon/h=o(1)$ so that the preceding derivations remain valid. In other words, we require $\epsilon\ll h\ll1$, a possible choice being $h=\epsilon^{3/4}$, as picked by Kapitonov (1980). The contribution of $S_\epsilon^{(v)}$ reduces to $-\psi(\boldsymbol{x})$, and we finally obtain

$$\lim_{\epsilon\to0}\int_{S_\epsilon}\left[G(\boldsymbol{x}-\boldsymbol{x}')\left(N^2\frac{\partial}{\partial n_h'}-\omega^2\frac{\partial}{\partial n'}\right)\psi(\boldsymbol{x}')\right.$$
$$\left.-\psi(\boldsymbol{x}')\left(N^2\frac{\partial}{\partial n_h'}-\omega^2\frac{\partial}{\partial n'}\right)G(\boldsymbol{x}-\boldsymbol{x}')\right]\mathrm{d}^2S'=-\psi(\boldsymbol{x}), \tag{7.7}$$

yielding (3.4*a*).

When $\boldsymbol{x}$ is situated on S, we write

$$\left(\int_{S_\epsilon}+\int_{S\setminus D_\epsilon}\right)\left[G(\boldsymbol{x}-\boldsymbol{x}')\left(N^2\frac{\partial}{\partial n_h'}-\omega^2\frac{\partial}{\partial n'}\right)\psi(\boldsymbol{x}')\right.$$
$$\left.-\psi(\boldsymbol{x}')\left(N^2\frac{\partial}{\partial n_h'}-\omega^2\frac{\partial}{\partial n'}\right)G(\boldsymbol{x}-\boldsymbol{x}')\right]\mathrm{d}^2S'=0, \tag{7.8}$$

where S_ϵ is the part of the preceding small cylinder situated outside S, up to its intersection with S, delimiting a small domain D_ϵ on S, and $S\setminus D_\epsilon$ is the rest of S with D_ϵ removed, as shown in figure 4(*b*).

We introduce Cartesian coordinates (x'', y'', z'') on S_ϵ, with the x''-axis in the vertical plane containing the line of steepest ascent through $\boldsymbol{x}$ on S, and the y''-axis along the level line. Assuming for definiteness the outward normal $\boldsymbol{n}$ at $\boldsymbol{x}$ to be directed upward at the angle θ the vertical, the tangent plane has the equation $z'' = -x'' \tan\theta = -r_h'' \tan\theta \cos\phi''$. The integral over $S_\epsilon^{(h)}$ is unchanged, while the integral over $S_\epsilon^{(v)}$ comprises two parts: one for z'' varying from 0 to h, and the other for z'' varying from $-r_h'' \tan\theta \cos\phi''$ to 0. This second part cancels out by integration over ϕ'', and we obtain half the integral over the complete small cylinder, namely

$$\lim_{\epsilon\to 0} \int_{S_\epsilon} \left[G(\boldsymbol{x}-\boldsymbol{x}') \left(N^2 \frac{\partial}{\partial n_h'} - \omega^2 \frac{\partial}{\partial n'} \right) \psi(\boldsymbol{x}') \right.$$
$$\left. - \psi(\boldsymbol{x}') \left(N^2 \frac{\partial}{\partial n_h'} - \omega^2 \frac{\partial}{\partial n'} \right) G(\boldsymbol{x}-\boldsymbol{x}') \right] \mathrm{d}^2 S' = -\frac{1}{2}\psi(\boldsymbol{x}). \tag{7.9}$$

Alternatively, we might simply point out, as did Kapitonov (1980), that the tangent plane divides the complete cylinder into two parts which are mirror images of each other through the horizontal plane; given the symmetry of the integrand, this implies that the integral over each part is equal to half its value for the complete cylinder.

To evaluate the integral over $S \setminus D_\epsilon$, we adapt the procedure of Martin (2006, § 5.5 and Appendix F). On D_ϵ, we have

$$0 < r_h'' < \epsilon, \quad 0 < \phi'' < 2\pi, \quad \mathrm{d}^2 S' = \frac{r_h''\, \mathrm{d}r_h''\, \mathrm{d}\phi''}{\cos\theta}. \tag{7.10a–c}$$

As $\epsilon \to 0$, hence $r_h'' \to 0$, the domain D_ϵ reduces, to leading order, to a small elliptic disc on the tangent plane to S at $\boldsymbol{x}$. To the next order, we write

$$z'' = -r_h'' \tan\theta \cos\phi'' + O(r_h''^2), \quad \boldsymbol{n}' = \boldsymbol{n} + O(r_h''), \quad \boldsymbol{x}'' \cdot \boldsymbol{n}' = O(r_h''^2), \tag{7.11a–c}$$

so that

$$G(\boldsymbol{x}'') = O(1/r_h''), \quad \boldsymbol{u}_G(\boldsymbol{x}'') \cdot \boldsymbol{n}' = O(1/r_h''). \tag{7.12a,b}$$

The integral over D_ϵ is seen to converge at $r_h'' = 0$ and to vanish as $\epsilon \to 0$. The integral over $S \setminus D_\epsilon$ becomes one over the entirety of S and, though improper, converges at $\boldsymbol{x}' = \boldsymbol{x}$.

We thus obtain

$$\int_S \left[G(\boldsymbol{x}-\boldsymbol{x}') \left(N^2 \frac{\partial}{\partial n_h'} - \omega^2 \frac{\partial}{\partial n'} \right) \psi(\boldsymbol{x}') - \psi(\boldsymbol{x}') \left(N^2 \frac{\partial}{\partial n_h'} - \omega^2 \frac{\partial}{\partial n'} \right) G(\boldsymbol{x}-\boldsymbol{x}') \right] \mathrm{d}^2 S'$$
$$= \frac{1}{2}\psi(\boldsymbol{x}) \quad (\boldsymbol{x} \in S). \tag{7.13}$$

Since the integral is convergent, the factor $1/2$ on the right-hand side is independent of the shape of the small vicinity of $\boldsymbol{x}$ involved in its derivation, either hemispherical for Martin & Llewellyn Smith (2012) or cylindrical here. Indeed, the complicated factor derived by Martin & Llewellyn Smith may be shown numerically, if not analytically, to evaluate to 0.5 for any values of the frequency ratio $\omega/N > 1$ and inclination θ of the normal $\boldsymbol{n}$ to the vertical, as seen in Appendix C.

7.2. *Layer potentials*

This result for the Kirchhoff–Helmholtz integral may be extended to the layer potentials by the method of Courant & Hilbert (1962, § IV.1.4). For this, we consider the double-layer

potential (3.10) and continue the dipole density μ as a twice continuously differentiable function into V_+, subject to the condition that $(N^2\partial/\partial n_h - \omega^2\partial/\partial n)\mu = 0$ on S; we then apply Green's theorem (3.2) inside V_+, choosing $f = \mu(\boldsymbol{x}')$ and $g = G(\boldsymbol{x} - \boldsymbol{x}')$. We obtain

$$\int_{V_+} G(\boldsymbol{x} - \boldsymbol{x}')(N^2\nabla_h'^2 - \omega^2\nabla'^2)\mu(\boldsymbol{x}')\,\mathrm{d}^3x'$$

$$= \mu(\boldsymbol{x}) + \psi_d(\boldsymbol{x}) \quad (\boldsymbol{x} \in V_+), \tag{7.14a}$$

$$= \frac{1}{2}\mu(\boldsymbol{x}) + \int_S \mu(\boldsymbol{x}')\left(N^2\frac{\partial}{\partial n_h'} - \omega^2\frac{\partial}{\partial n'}\right)G(\boldsymbol{x} - \boldsymbol{x}')\,\mathrm{d}^2S' \quad (\boldsymbol{x} \in S), \tag{7.14b}$$

$$= \psi_d(\boldsymbol{x}) \quad (\boldsymbol{x} \in V_-). \tag{7.14c}$$

The volume integral on the left-hand side is a continuous function of $\boldsymbol{x}$ across S, implying, as $\boldsymbol{x}$ approaches S from either V_+ or V_-, that

$$\psi_d(\boldsymbol{x} \in S_\pm) = \mp\frac{1}{2}\mu(\boldsymbol{x}) + \int_S \mu(\boldsymbol{x}')\left(N^2\frac{\partial}{\partial n_h'} - \omega^2\frac{\partial}{\partial n'}\right)G(\boldsymbol{x} - \boldsymbol{x}')\,\mathrm{d}^2S', \tag{7.15}$$

consistent with (6.6).

We proceed in the same way for the single-layer potential (3.7), continuing the monopole density σ as a twice continuously differentiable function into V_+, subject to the condition that $(N^2\partial/\partial n_h - \omega^2\partial/\partial n)\sigma = 0$ on S, then applying (3.2) inside V_+ with $f = \sigma(\boldsymbol{x}')$ and $g = G(\boldsymbol{x} - \boldsymbol{x}')$. Taking the derivative $N^2\partial/\partial n_h - \omega^2\partial/\partial n$ of both sides of the result, and letting $\boldsymbol{x}$ approach S from either V_+ or V_-, we obtain

$$\left(N^2\frac{\partial}{\partial n_h} - \omega^2\frac{\partial}{\partial n}\right)\psi_s(\boldsymbol{x} \in S_\pm) = \pm\frac{1}{2}\sigma(\boldsymbol{x})$$

$$- \int_S \sigma(\boldsymbol{x}')\left(N^2\frac{\partial}{\partial n_h'} - \omega^2\frac{\partial}{\partial n'}\right)G(\boldsymbol{x} - \boldsymbol{x}')\,\mathrm{d}^2S', \tag{7.16}$$

consistent with (6.3).

8. Far field

At this stage one question remains, the contribution of the surface S_∞ at infinity, assumed to vanish in the derivation of the Kirchhoff–Helmholtz integral (3.4). To answer it, we use the studies of the far field by Voisin (2003) and Martin & Llewellyn Smith (2012).

Consider a sphere S_R of large radius R, with centre within the oscillating body, and evaluate its contribution

$$\int_{S_R} [\boldsymbol{u}(\boldsymbol{x}') \cdot \boldsymbol{n}' G(\boldsymbol{x}' - \boldsymbol{x}) - \psi(\boldsymbol{x}')\boldsymbol{u}_G(\boldsymbol{x}' - \boldsymbol{x}) \cdot \boldsymbol{n}']\,\mathrm{d}^2S' \tag{8.1}$$

as $R \to \infty$. The Green's function satisfies

$$G(\boldsymbol{x}' - \boldsymbol{x}) = O\left(\frac{1}{R}\right), \quad \boldsymbol{u}_G(\boldsymbol{x}' - \boldsymbol{x}) = O\left(\frac{1}{R^2}\right). \tag{8.2a,b}$$

In the evanescent frequency range $\omega > N$, the far-field studies give for the layer potentials the decay laws

$$\psi(\boldsymbol{x}') = O\left(\frac{1}{R}\right), \quad \boldsymbol{u}(\boldsymbol{x}') = O\left(\frac{1}{R^2}\right). \tag{8.3a,b}$$

Provided the waves decay at the same rate, and given the surface area element d^2S' grows as R^2, the contribution of S_R is seen to vary as $1/R$ and to vanish as $R \to \infty$.

In the propagating frequency range $0 < \omega < N$, different decay laws are obtained depending on whether we are inside or outside the wave beams, delimited by the critical rays tangential to S. Outside the beams the decay laws are the same as before, (8.3) for the layer potentials. Provided the waves decay at the same rate, the contribution of that part of S_R vanishes as $R \to \infty$. Inside the beams the decay laws become, for the layer potentials,

$$\psi(\boldsymbol{x}') = O\left(\frac{1}{R^{1/2}}\right), \quad \boldsymbol{u}(\boldsymbol{x}') = O\left(\frac{1}{R^{1/2}}\right), \tag{8.4a,b}$$

while the associated part of S_R has its area varying as R. Provided the waves decay at the same rate, the contribution of this part of S_R varies as $1/R^{1/2}$ and vanishes as $R \to \infty$.

Accordingly, the decay laws (8.3) and (8.4) must be taken as Sommerfeld-type radiation conditions, to be satisfied by the waves in order to ensure that they all emanate from the oscillating body and do not come in from infinity.

9. Conclusion

Two boundary integral formulations have been presented for the generation of monochromatic internal waves by an oscillating body in an inviscid stratified fluid. One formulation is direct, involves both single and double layers through the Kirchhoff–Helmholtz integral (3.6), and leads to the integral equation (3.5). The other formulation is indirect, involves the single layer (3.7) alone, and leads to the integro-differential equation (6.11). A method for the analytical solution of these equations has been proposed, in two steps: first, in the frequency range of evanescent waves, the horizontal and vertical coordinates are stretched according to (3.17), transforming the wave equation into a Poisson equation to which the usual methods can be applied; and second, the solution is continued analytically to the frequency range of propagating waves, using the causality condition that the waves be analytic, for time dependence as $\exp(-\mathrm{i}\omega t)$ say, in the upper half of the complex ω-plane, a continuation implemented via Lighthill's radiation condition (3.18).

The method has been applied to the two-dimensional case of an elliptic cylinder in § 4 and the three-dimensional case of a spheroid in § 5. Arbitrary oscillations have been considered, and the results specialized to radial pulsations and rigid vibrations. For these, the results for the waves are gathered in tables 3 and 4, and those for the distributions of singularities equivalent to the body in table 5. The success of the method comes from the existence, in the stretched coordinates, of a separated expansion of the Green's function in eigenfunctions for the given geometry: circular functions for the cylinder, and spherical harmonics for the spheroid. As a result, the boundary integral equation reduces to a diagonal (infinite) linear system, solved analytically. Sturova (2001), for the cylinder, used a similar expansion but without coordinate stretching; the circular functions were not eigenfunctions, yielding a non-diagonal system solved numerically by truncation.

The waves for arbitrary oscillations of the cylinder are obtained as an expansion of the general form anticipated by Barcilon & Bleistein (1969) and Hurley (1972). They involve complex stretched coordinates, which Lighthill's radiation condition allows to be written as simple combinations of the characteristic coordinates x_+ and x_-, with the determination of these multivalued combinations set unequivocally.

The greatest interest of the boundary integral method lies, however, elsewhere; namely, in the determination of a distribution of singularities equivalent to the oscillating body. First, this distribution allows the effect of viscosity to be added into the theory. Inviscid waves are but a web of singular critical rays, at which the amplitude diverges and the phase jumps; it is viscosity, acting locally to smooth out the singularities, which determines the

distribution of the waves into space and sets ultimately their amplitude and their phase. The mathematical description of this process takes place in Fourier space, as shown by Lighthill (1978, § 4.10) at large distances from the forcing and Voisin (2020) at arbitrary distance from it. The knowledge of a representation of the body as a distribution of singularities, and thence of its spectrum, provides the basis for this description; it avoids the need, as did Hurley (1997) and Hurley & Keady (1997), to calculate the inviscid waves first, then derive their Fourier representation and finally add viscous attenuation into it.

The representations of the vibrating elliptic cylinder and sphere in table 5 have been applied by Voisin (2020) and Voisin *et al.* (2011), respectively, to the calculation of their waves and compared successfully with experiment. The effect of viscosity is illustrated in figure 5 for the vertical vibrations at the frequency ω and velocity $W = -\omega A$, with $\omega_0/N = 0.44$ and $A = 0.32$ cm, of a cylinder of horizontal semi-axis $a = 2.52$ cm, vertical semi-axis $b = 0.86$ cm and aspect ratio $a/b \approx 3$ in a fluid of buoyancy frequency $N = 0.97\ \mathrm{s}^{-1}$ and kinematic viscosity $\nu = 1\ \mathrm{mm}^2\ \mathrm{s}^{-1}$, corresponding to the measurements in figure 8(d) of Sutherland & Linden (2002). The plotted quantity is the amplitude of the time derivative of the buoyancy frequency disturbance, $N_t^2 = -N^2 \partial u_z/\partial z$, normalized by

$$A_{N_t^2} = N^3 \frac{aA}{2c^2} \sin\theta_0 \cos^2\theta_0. \tag{9.1}$$

The inviscid expression for this quantity, derived from table 3, is

$$\frac{N_t^2}{A_{N_t^2}} = \exp(\mathrm{i}\eta_0) \left\{ \frac{c^3}{[(x_- - \mathrm{i}0\,\mathrm{sign}\,\zeta_-)^2 - c^2]^{3/2}} - \frac{c^3}{[(x_+ + \mathrm{i}0\,\mathrm{sign}\,\zeta_+)^2 - c^2]^{3/2}} \right\}, \tag{9.2}$$

and its viscous expression, derived from (6.23), is

$$\frac{N_t^2}{A_{N_t^2}} = -\mathrm{i}c^2 \exp(\mathrm{i}\eta_0) \sum_{\pm} \mathrm{sign}\,\zeta_\pm \int_0^\infty \kappa\, \mathrm{J}_1(\kappa c) \exp\left(-\beta\kappa^3 \frac{d}{c}|\zeta_\pm|\right) \times \exp(\pm\mathrm{i}\kappa x_\pm\, \mathrm{sign}\,\zeta_\pm)\, \mathrm{d}\kappa. \tag{9.3}$$

Both expressions are plotted in figure 5. To better illustrate the structure of the waves, in particular the occurrence of singularities at critical points on the cylinder, they are plotted not only in the fluid but also inside the body. Inviscid dynamics is seen to provide a wave skeleton, which is then fleshed out by viscous diffusion.

Another application of the distribution of singularities is, for a rigid body, the determination of the added mass of the body. The added mass follows from the first moment of the distribution, and provides direct access to the energy radiated by the body and to the force exerted on it, without requiring the actual calculation of the waves. The energy is important for oceanic applications, as it characterizes the conversion rate from the barotropic tide oscillating over bottom topography to the internal tide that this oscillation generates; and the force is important for the stability of midwater floats, as it governs their oscillation back to their neutral buoyancy level once displaced away from it then released. These aspects will be considered separately; a summary presentation may be found in Voisin (2009).

Coming back to the foundations of the boundary integral method, it must be noted that the derivations in §§ 3 and 7 have all been made for evanescent waves, of frequency $\omega > N$. For these, the only singularities in the boundary integrals arise when the observation point P is on the surface S. For propagating waves, of frequency $0 < \omega < N$, the situation is different: singularities are present whenever P is inside a wave beam, delimited by the critical rays tangential to S, and they take place at one or several closed curves where

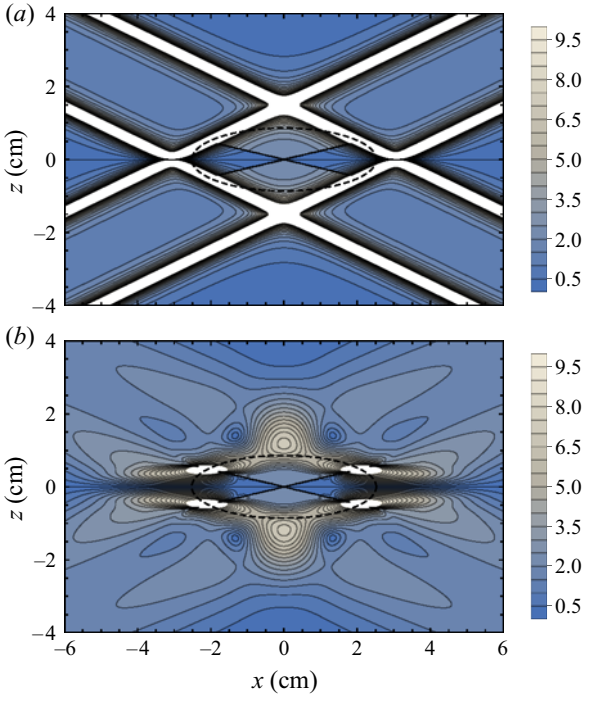

Figure 5. Waves for the elliptic cylinder in figure 8(*d*) of Sutherland & Linden (2002), as predicted (*a*) in an inviscid fluid by (9.2) and (*b*) in a viscous fluid by (9.3). The predictions are plotted both outside and inside the cylinder, whose outline is shown dashed.

the double cone with apex at P, vertical axis and semi-aperture θ_0 intersects S. Martin & Llewellyn Smith (2012) considered this frequency range in detail, paying particular attention to the far field, to which the present § 8 is devoted. It is beyond our scope to investigate this frequency range further. As a rule, we expect those of our conclusions that do not involve the frequency explicitly to hold whatever the frequency.

One such conclusion concerns the possibility of replacing the direct approach of § 3, representing the oscillating body as a combination of single and double layers, by the indirect approach of § 6, involving a single layer alone. For generation problems, this possibility requires the existence of a fictitious flow inside the body, imagined to be filled with fluid, simultaneously satisfying the wave equation throughout the body and the continuity of the pressure at its boundary. The elliptic cylinder and the spheroid in §§ 4 and 5, symmetric with respect to the horizontal and vertical directions, may be treated by both approaches; an elliptic cylinder with inclined axes requires, however, the direct approach. For scattering problems, Martin & Llewellyn Smith (2012) showed that a double layer always suffices.

Another conclusion concerns the values of the boundary integrals at the boundary. For the Kirchhoff–Helmholtz integral (7.13), the same arithmetic mean $\psi(\boldsymbol{x})/2$ between the values $\psi(\boldsymbol{x})$ and 0 of the integral (3.4) on either side of the boundary is obtained as for the Laplace and Helmholtz equations. Similarly, the same additional term $\pm\mu(\boldsymbol{x})/2$, with $\mu(\boldsymbol{x})$ the dipole density, is obtained for the double-layer potential (7.15) when the boundary is approached from either side, and the same additional term $\pm\sigma(\boldsymbol{x})/2$, with $\sigma(\boldsymbol{x})$ the monopole density, for the modified normal derivative (7.16) of the single-layer potential.

It is unclear at this stage how boundary elements would be implemented numerically for internal waves in a three-dimensional setting. All existing numerical implementations are two-dimensional and deal with vertically trapped waves, decomposed into a series of normal modes. Sturova (2006, 2011) considers a cylinder, either circular or elliptic, and uses an indirect single-layer representation for $0 < \omega < N$ and a direct Kirchhoff–Helmholtz representation for $\omega > N$; she does not discuss, however, how the contour of the cylinder is decomposed into elements, nor the way the weak singularities of the kernels are processed. Pétrélis *et al.* (2006) consider various topographies and use straight elements, discretized with respect to the vertical coordinate; Balmforth & Peacock (2009), Echeverri & Peacock (2010), Echeverri *et al.* (2011) and Mathur *et al.* (2014) do the same but discretize the elements with respect to the horizontal coordinate. The topographies are represented as single layers and the weak singularities of the kernels are eliminated by integrating the integral equations along each element. Clearly, the boundary element method for three-dimensional internal waves remains a topic for further investigation.

Acknowledgements. This research was initiated at DAMTP under the supervision of D. Crighton in 1998, and continued at LEGI where it benefitted from the input of A. Chikhi during a master internship in 2005 and from conversations with S. Llewellyn Smith and A. Davis during a stay at UCSD in 2008. N. Shmakova is thanked for kindly translating the obituary by Sveshnikov *et al.* (1989), and E. Ermanyuk for clarifying the translation of Sobolev (1954). Application of the boundary integral method to monochromatic internal waves was suggested by V. Gorodtsov at the Institute for Problems in Mechanics in Moscow on 26 May 1998, during a marathon conversation organized by Y. Chashechkin with S. Smirnov acting as a translator. One anonymous reviewer is thanked for pointing out several misconceptions about boundary integrals in the original manuscript and, together with the editor, for thoughtful suggestions which led to redesign and improvement of the paper.

Funding. This work was supported by Marie Curie grant ERBFMBI CT97 2653 (1998) from the European Commission, grants TOPOGI-3D (2005–2008) and PIWO (2008–2011) from the French National Research Agency (ANR), and a grant from Fondation Simone et Cino Del Duca–Institut de France (2015–2018).

Declaration of interests. The authors report no conflict of interest.

Author ORCIDs.
Bruno Voisin https://orcid.org/0000-0002-3741-3840.

Appendix A. Legendre functions

The ordinary Legendre functions $P_l(z)$ and $Q_l(z)$ of non-negative integer degree l are defined in the plane of the complex variable z, cut along the real interval $[-1, 1]$, as

$$P_l(z) = \frac{1}{(2l)!!}\frac{\mathrm{d}^l}{\mathrm{d}z^l}(z^2-1)^l, \tag{A1a}$$

$$Q_l(z) = \frac{1}{(2l)!!}\frac{\mathrm{d}^l}{\mathrm{d}z^l}\left[(z^2-1)^l \ln\left(\frac{z+1}{z-1}\right)\right] - \frac{1}{2}P_l(z)\ln\left(\frac{z+1}{z-1}\right). \tag{A1b}$$

The associated Legendre functions $P_l^m(z)$ and $Q_l^m(z)$ are defined for non-negative integer order m as

$$P_l^m(z) = (z^2-1)^{m/2}\frac{\mathrm{d}^m}{\mathrm{d}z^m}P_l(z), \quad Q_l^m(z) = (z^2-1)^{m/2}\frac{\mathrm{d}^m}{\mathrm{d}z^m}Q_l(z), \tag{A2a,b}$$

and for negative order as

$$P_l^{-m}(z) = \frac{(l-m)!}{(l+m)!}P_l^m(z), \quad Q_l^{-m}(z) = \frac{(l-m)!}{(l+m)!}Q_l^m(z). \tag{A3a,b}$$

On the cut $[-1, 1]$, the Legendre functions are also called Ferrers functions. The ordinary functions $\mathrm{P}_l(x)$ and $\mathrm{Q}_l(x)$ of the real variable $x \in [-1, 1]$ are defined for degree l as

$$\mathrm{P}_l(x) = \frac{1}{(2l)!!}\frac{\mathrm{d}^l}{\mathrm{d}x^l}(x^2-1)^l, \tag{A4a}$$

$$\mathrm{Q}_l(x) = \frac{1}{(2l)!!}\frac{\mathrm{d}^l}{\mathrm{d}x^l}\left[(x^2-1)^l \ln\left(\frac{1+x}{1-x}\right)\right] - \frac{1}{2}\mathrm{P}_l(x)\ln\left(\frac{1+x}{1-x}\right), \tag{A4b}$$

and the associated functions $\mathrm{P}_l^m(x)$ and $\mathrm{Q}_l^m(x)$ are defined for positive order m as

$$\mathrm{P}_l^m(x) = (-1)^m(1-x^2)^{m/2}\frac{\mathrm{d}^m}{\mathrm{d}x^m}\mathrm{P}_l(x), \quad \mathrm{Q}_l^m(x) = (-1)^m(1-x^2)^{m/2}\frac{\mathrm{d}^m}{\mathrm{d}x^m}\mathrm{Q}_l(x), \tag{A5a,b}$$

and for negative order as

$$\mathrm{P}_l^{-m}(x) = (-1)^m\frac{(l-m)!}{(l+m)!}\mathrm{P}_l^m(x), \quad \mathrm{Q}_l^{-m}(x) = (-1)^m\frac{(l-m)!}{(l+m)!}\mathrm{Q}_l^m(x). \tag{A6a,b}$$

The two types of functions are related to each other at the cut by

$$P_l^m(x \pm \mathrm{i}0) = (\mp\mathrm{i})^m\,\mathrm{P}_l^m(x), \quad Q_l^m(x \pm \mathrm{i}0) = (\mp\mathrm{i})^m\left(\mathrm{Q}_l^m \mp \mathrm{i}\frac{\pi}{2}\mathrm{P}_l^m\right)(x). \tag{A7a,b}$$

Several definitions and notations of the Legendre functions exist in the literature. The above definitions and notations are based on Hobson (1931, chapters 2, 3 and 5), Abramowitz & Stegun (1972, chapter 8) and Olver *et al.* (2010, chapter 14).

The derivations in § 5 use the symmetry relations

$$P_l^m(-z) = (-1)^l P_l^m(z), \quad Q_l^m(-z) = (-1)^{l+1}Q_l^m(z), \tag{A8a,b}$$

and

$$\mathrm{P}_l^m(-x) = (-1)^{l+m}\,\mathrm{P}_l^m(x), \quad \mathrm{Q}_l^m(-x) = (-1)^{l+m+1}\,\mathrm{Q}_l^m(x), \tag{A9a,b}$$

the recurrence relations

$$(z^2-1)^{1/2}\frac{\mathrm{d}}{\mathrm{d}z}P_l^m(z) = P_l^{m+1}(z) + m\frac{z}{(z^2-1)^{1/2}}P_l^m(z), \tag{A10}$$

and

$$(1-x^2)^{1/2}\frac{\mathrm{d}}{\mathrm{d}x}\mathrm{P}_l^m(x) = -\,\mathrm{P}_l^{m+1}(x) - m\frac{x}{(1-x^2)^{1/2}}\mathrm{P}_l^m(x), \tag{A11}$$

with $Q_l^m(z)$ satisfying the same relations as $P_l^m(z)$, and $\mathrm{Q}_l^m(x)$ as $\mathrm{P}_l^m(x)$, and the identities

$$P_l^m(z)Q_l^{m+1}(z) - P_l^{m+1}(z)Q_l^m(z) = -\frac{(-1)^m}{(z^2-1)^{1/2}}\frac{(l+m)!}{(l-m)!}, \tag{A12}$$

and

$$\mathrm{P}_l^m(x)\,\mathrm{Q}_l^{m+1}(x) - \mathrm{P}_l^{m+1}(x)\,\mathrm{Q}_l^m(x) = -\frac{1}{(1-x^2)^{1/2}}\frac{(l+m)!}{(l-m)!}. \tag{A13}$$

Gegenbauer's finite integral in § 12.14 of Watson (1944) is also used, in the form

$$\int_0^\pi \exp(\mathrm{i}z\cos\theta\cos\alpha)\,\mathrm{J}_m(z\sin\theta\sin\alpha)\,\mathrm{P}_l^m(\cos\theta)\sin\theta\,\mathrm{d}\theta = 2\mathrm{i}^{l-m}\,\mathrm{j}_l(z)\,\mathrm{P}_l^m(\cos\alpha), \tag{A14}$$

with $\mathrm{J}_m(z)$ a cylindrical Bessel function and $\mathrm{j}_l(z)$ a spherical Bessel function.

Appendix B. Spherical harmonics

Spherical harmonics are defined in terms of associated Legendre functions as

$$Y_l^m(\theta,\phi)=\sqrt{\frac{2l+1}{4\pi}\frac{(l-m)!}{(l+m)!}}\,\mathrm{P}_l^m(\cos\theta)\exp(\mathrm{i}m\phi), \tag{B1}$$

with l a non-negative integer and m an integer such that $|m|\leqslant l$; see for example Jackson (1999, § 3.5) and Olver *et al.* (2010, § 14.30). They form a complete orthonormal set over the surface of the unit sphere, in terms of which an arbitrary function $g(\theta,\phi)$ may be expanded as

$$g(\theta,\phi)=\sum_{l=0}^{\infty}\sum_{m=-l}^{l}g_{lm}Y_l^m(\theta,\phi), \tag{B2}$$

with coefficients

$$g_{lm}=\int g(\theta,\phi)\overline{Y_l^m(\theta,\phi)}\,\mathrm{d}\Omega, \tag{B3}$$

where an overbar denotes a complex conjugate and $\mathrm{d}\Omega=\sin\theta\,\mathrm{d}\theta\,\mathrm{d}\phi$ the solid angle element.

Appendix C. Another look at boundary values

When $\boldsymbol{x}$ is on S and the Kirchhoff–Helmholtz integral is evaluated on a small surface surrounding it, Martin & Llewellyn Smith (2012) used a hemisphere H_ϵ of radius ϵ with its polar axis along the normal $\boldsymbol{n}$ to S at $\boldsymbol{x}$. Introducing spherical polar coordinates (r'',θ'',ϕ'') with the same polar axis (so that ϕ'' differs from that in § 7.1), we have

$$r''=\epsilon,\quad 0<\theta''<\pi/2,\quad 0<\phi''<2\pi,\quad \boldsymbol{n}'=\boldsymbol{e}_{r''},\quad \mathrm{d}^2S'=\epsilon^2\sin\theta''\,\mathrm{d}\theta''\,\mathrm{d}\phi'', \tag{C1a–e}$$

yielding

$$\int_{H_\epsilon}G(\boldsymbol{x}'')\,\mathrm{d}^2S'=\frac{\epsilon}{4\pi\omega^2(1-\Gamma^2)^{1/2}}\int_0^{2\pi}\mathrm{d}\phi''\int_0^{\pi/2}\frac{\sin\theta''\,\mathrm{d}\theta''}{[\Lambda(\theta'',\phi'';\theta,\Gamma)]^{1/2}}, \tag{C2a}$$

$$\int_{H_\epsilon}\boldsymbol{u}_G(\boldsymbol{x}'')\cdot\boldsymbol{n}'\,\mathrm{d}^2S'=\frac{(1-\Gamma^2)^{1/2}}{4\pi}\int_0^{2\pi}\mathrm{d}\phi''\int_0^{\pi/2}\frac{\sin\theta''\,\mathrm{d}\theta''}{[\Lambda(\theta'',\phi'';\theta,\Gamma)]^{3/2}}, \tag{C2b}$$

where $\Gamma=N/\omega$, with $0<\Gamma<1$, and

$$\Lambda(\theta'',\phi'';\theta,\Gamma)=1-\Gamma^2(\sin\theta\sin\theta''\cos\phi''-\cos\theta\cos\theta'')^2. \tag{C3}$$

As $\epsilon\to0$ the same result (7.9) is obtained as for the cutoff vertical cylinder S_ϵ in figure 4(*b*), but with the factor $1/2$ on the right-hand side replaced by the right-hand side of (C2*b*).

Now, as seen in § 7.1, the two integrals over S_ϵ and H_ϵ must have the same limit as $\epsilon\to0$. Numerically, the right-hand side of (C2*b*) evaluates to 0.5 whatever the values of Γ and θ. Analytically, it evaluates to $1/2$ for $\Gamma=0$, independent of θ, but the extension of this result to arbitrary Γ and θ has not been possible. We may, however, remark, as for S_ϵ following (7.9), that the tangent plane to S at $\boldsymbol{x}$ divides a sphere of radius ϵ around $\boldsymbol{x}$ into two hemispheres which are mirror images of each other through the horizontal plane, and that the symmetry of the integrand is such that each hemisphere gives half the integral over the complete sphere, shown by Martin & Llewellyn Smith (2012) to evaluate to 1.

References

Abramowitz, M. & Stegun, I.A. 1972 *Handbook of Mathematical Functions*, 10th edn. Dover.

Allakhverdiev, K.B. & Pletner, Y.D. 1993 A fundamental solution of the two-dimensional operator of gravity-gyroscopic waves and some initial-boundary problems. *Phys. Dokl.* **38**, 234–236.

Appleby, J.C. & Crighton, D.G. 1986 Non-Boussinesq effects in the diffraction of internal waves from an oscillating cylinder. *Q. J. Mech. Appl. Maths* **39**, 209–231.

Appleby, J.C. & Crighton, D.G. 1987 Internal gravity waves generated by oscillations of a sphere. *J. Fluid Mech.* **183**, 439–450.

Backus, G. & Rieutord, M. 2017 Completeness of inertial modes of an incompressible inviscid fluid in a corotating ellipsoid. *Phys. Rev.* E **95**, 053116.

Balmforth, N.J. & Peacock, T. 2009 Tidal conversion by supercritical topography. *J. Phys. Oceanogr.* **39**, 1965–1974.

Barcilon, V. & Bleistein, N. 1969 Scattering of inertial waves in a rotating fluid. *Stud. Appl. Maths* **48**, 91–104.

Bardakov, R.N., Vasil'ev, A.Y. & Chashechkin, Y.D. 2007 Calculation and measurement of conical beams of three-dimensional periodic internal waves excited by a vertically oscillating piston. *Fluid Dyn.* **42**, 612–626.

Bleistein, N. 1984 *Mathematical Methods for Wave Phenomena*. Academic.

Brebbia, C.A., Telles, J.C.F. & Wrobel, L.C. 1984 *Boundary Element Techniques*. Springer.

Brouzet, C., Ermanyuk, E.V., Moulin, M., Pillet, G. & Dauxois, T. 2017 Added mass: a complex facet of tidal conversion at finite depth. *J. Fluid Mech.* **831**, 101–127.

Bryan, G.H. 1889 The waves on a rotating liquid spheroid of finite ellipticity. *Phil. Trans. R. Soc. Lond.* A **180**, 187–219.

Cayley, A. 1870 On the geodesic lines on an oblate spheroid. *Phil. Mag.* **40**, 329–340.

Cheng, A.H.-D. & Cheng, D.T. 2005 Heritage and early history of the boundary element method. *Engng Anal. Bound. Elem.* **29**, 268–302.

Copley, L.G. 1968 Fundamental results concerning integral representations in acoustic radiation. *J. Acoust. Soc. Am.* **44**, 28–32.

Courant, R. & Hilbert, D. 1962 *Methods of Mathematical Physics*, vol. II. Wiley.

Crighton, D.G., Dowling, A.P., Ffowcs Williams, J.E., Heckl, M. & Leppington, F.G. 1992 *Modern Methods in Analytical Acoustics*. Springer.

Davis, A.M.J. 2012 Generation of internal waves from rest: extended use of complex coordinates, for a sphere but not a disk. *J. Fluid Mech.* **703**, 374–390.

Davis, A.M.J. & Llewellyn Smith, S.G. 2010 Tangential oscillations of a circular disk in a viscous stratified fluid. *J. Fluid Mech.* **656**, 342–359.

Davydova, M.A. 2004 Asymptotic behavior of a boundary layer solution to one hydrodynamic problem. *Comp. Maths Math. Phys.* **44**, 1038–1050.

Davydova, M.A. 2006*a* On the dynamic potential theory for the equation of a weakly stratified fluid. *Differ. Equ.* **42**, 537–547.

Davydova, M.A. 2006*b* Asymptotic solution of the problem on nonstationary vibrations of a continuously stratified medium with small dissipation. *Differ. Equ.* **42**, 1623–1632.

Davydova, M.A. & Chashechkin, Y.D. 2004 The structure of three-dimensional periodic boundary layers in a continuously stratified fluid. *J. Appl. Maths Mech.* **68**, 391–397.

Echeverri, P. & Peacock, T. 2010 Internal tide generation by arbitrary two-dimensional topography. *J. Fluid Mech.* **659**, 247–266.

Echeverri, P., Yokossi, T., Balmforth, N.J. & Peacock, T. 2011 Tidally generated internal-wave attractors between double ridges. *J. Fluid Mech.* **669**, 354–374.

Ermanyuk, E.V. 2002 The rule of affine similitude for the force coefficients of a body oscillating in a uniformly stratified fluid. *Exp. Fluids* **32**, 242–251.

Ermanyuk, E.V. & Gavrilov, N.V. 2002 Oscillations of cylinders in a linearly stratified fluid. *J. Appl. Mech. Tech. Phys.* **43**, 503–511.

Ermanyuk, E.V. & Gavrilov, N.V. 2003 Force on a body in a continuously stratified fluid. Part 2. Sphere. *J. Fluid Mech.* **494**, 33–50.

Flynn, M.R., Onu, K. & Sutherland, B.R. 2003 Internal wave excitation by a vertically oscillating sphere. *J. Fluid Mech.* **494**, 65–93.

Gabov, S.A. 1984*a* Explicit solution and existence of a limiting amplitude for a problem in the dynamics of a stratified fluid. *Sov. Maths Dokl.* **30**, 190–194.

Gabov, S.A. 1984*b* The angular potential for an equation of S.L. Sobolev and its applications. *Sov. Maths Dokl.* **30**, 405–409.

GABOV, S.A. 1985 The solution of a problem of stratified fluid dynamics and its stabilization as $t \to \infty$. *USSR Comp. Maths Math. Phys.* **25** (3), 47–55.

GABOV, S.A. & KRUTITSKII, P.A. 1987 On the non-stationary Larsen problem. *USSR Comp. Maths Math. Phys.* **27** (4), 148–154.

GABOV, S.A. & KRUTITSKII, P.A. 1989 On the small vibrations of a section placed at the boundary of separation between two stratified liquids. *USSR Comp. Maths Math. Phys.* **29** (2), 154–162.

GABOV, S.A., MALYSHEVA, G.Y. & SVESHNIKOV, A.G. 1983 A composite equation related to oscillations of a stratified compressible fluid. *Differ. Equ.* **19**, 866–873.

GABOV, S.A., MALYSHEVA, G.Y., SVESHNIKOV, A.G. & SHATOV, A.K. 1984 On some equations arising in the dynamics of a rotating stratified and compressible fluid. *USSR Comp. Maths Math. Phys.* **24** (6), 162–170.

GABOV, S.A. & MAMEDOV, K.S. 1983 The potential function and problems on oscillations of an exponentially stratified fluid. *Sov. Maths Dokl.* **27**, 309–312.

GABOV, S.A. & ORAZOV, B.B. 1986 The equation $(\partial^2/\partial t^2)[u_{xx} - u] + u_{xx} = 0$ and several problems associated with it. *USSR Comp. Maths Math. Phys.* **26** (1), 58–64.

GABOV, S.A. & PLETNER, Y.D. 1985 An initial-boundary value problem for the gravitational-gyroscopic wave equation. *USSR Comp. Maths Math. Phys.* **25** (6), 64–68.

GABOV, S.A. & PLETNER, Y.D. 1987*a* The gravitational-gyroscopic wave equation: the angular potential and its applications. *USSR Comp. Maths Math. Phys.* **27** (1), 66–73.

GABOV, S.A. & PLETNER, Y.D. 1987*b* Solvability of an exterior initial-boundary value problem for the gravitational gyroscopic wave equation. *USSR Comp. Maths Math. Phys.* **27** (3), 44–49.

GABOV, S.A. & PLETNER, Y.D. 1987*c* On the Dirichlet problem for the equation of gravitational-gyroscopic waves. *Sov. Maths Dokl.* **36**, 43–46.

GABOV, S.A. & PLETNER, Y.D. 1988 The problem of the oscillations of a flat disc in a stratified liquid. *USSR Comp. Maths Math. Phys.* **28** (1), 41–47.

GABOV, S.A. & SHEVTSOV, P.V. 1983 Basic boundary value problems for the equation of oscillations of a stratified fluid. *Sov. Maths Dokl.* **27**, 238–241.

GABOV, S.A. & SHEVTSOV, P.V. 1984 On a differential equation of the type of Sobolev's equation. *Sov. Maths Dokl.* **29**, 411–414.

GABOV, S.A. & SIMAKOV, S.T. 1989 The theory of internal and surface waves in a stratified liquid. *USSR Comp. Maths Math. Phys.* **29** (1), 155–164.

GARRETT, C. & KUNZE, E. 2007 Internal tide generation in the deep ocean. *Annu. Rev. Fluid Mech.* **39**, 57–87.

GAUL, L., KÖGL, M. & WAGNER, M. 2003 *Boundary Element Methods for Engineers and Scientists*. Springer.

GHAEMSAIDI, S.J. & PEACOCK, T. 2013 3D Stereoscopic PIV visualization of the axisymmetric conical internal wave field generated by an oscillating sphere. *Exp. Fluids* **54**, 1454.

GIBSON, W.C. 2014 *The Method of Moments in Electromagnetics*, 2nd edn. Chapman and Hall/CRC.

GORODTSOV, V. 2013 Small wave–vortex disturbances in stratified fluid. *Procedia IUTAM* **8**, 111–118.

GORODTSOV, V.A. & TEODOROVICH, E.V. 1980 On the generation of internal waves in the presence of uniform straight-line motion of local and nonlocal sources. *Izv. Atmos. Ocean. Phys.* **16**, 699–704.

GORODTSOV, V.A. & TEODOROVICH, E.V. 1982 Study of internal waves in the case of rapid horizontal motion of cylinders and spheres. *Fluid Dyn.* **17**, 893–898.

GRAY, E.P., HART, R.W. & FARRELL, R.A. 1983 The structure of the internal wave Mach front generated by a point source moving in a stratified fluid. *Phys. Fluids* **26**, 2919–2931.

HAPPEL, J. & BRENNER, H. 1983 *Low Reynolds Number Hydrodynamics*, 2nd edn. Springer.

HART, R.W. 1981 Generalized scalar potentials for linearized three-dimensional flows with vorticity. *Phys. Fluids* **24**, 1418–1420.

HENDERSHOTT, M.C. 1969 Impulsively started oscillations in a rotating stratified fluid. *J. Fluid Mech.* **36**, 513–527.

HINCH, E.J. 2020 *Think Before You Compute*. Cambridge University Press.

HOBSON, E.W. 1931 *The Theory of Spherical and Ellipsoidal Harmonics*. Cambridge University Press.

HURLEY, D.G. 1970 Internal waves in a wedge-shaped region. *J. Fluid Mech.* **43**, 97–120.

HURLEY, D.G. 1972 A general method for solving steady-state internal gravity wave problems. *J. Fluid Mech.* **56**, 721–740.

HURLEY, D.G. 1997 The generation of internal waves by vibrating elliptic cylinders. Part 1. Inviscid solution. *J. Fluid Mech.* **351**, 105–118.

HURLEY, D.G. & HOOD, M.J. 2001 The generation of internal waves by vibrating elliptic cylinders. Part 3. Angular oscillations and comparison of theory with recent experimental observations. *J. Fluid Mech.* **433**, 61–75.

HURLEY, D.G. & KEADY, G. 1997 The generation of internal waves by vibrating elliptic cylinders. Part 2. Approximate viscous solution. *J. Fluid Mech.* **351**, 119–138.

IVERS, D.J., JACKSON, A. & WINCH, D. 2015 Enumeration, orthogonality and completeness of the incompressible Coriolis modes in a sphere. *J. Fluid Mech.* **766**, 468–498.

JACKSON, J.D. 1999 *Classical Electrodynamics*, 3rd edn. Wiley.

KAPITONOV, B.V. 1980 Potential theory for the equation of small oscillations of a rotating fluid. *Maths USSR Sb.* **37**, 559–579.

KERSWELL, R.R. 1995 On the internal shear layers spawned by the critical regions in oscillatory Ekman boundary layers. *J. Fluid Mech.* **298**, 311–325.

KHARIK, V.M. 1993 Generation of internal waves in a rotating, stratified fluid: some symmetry properties. *J. Math. Phys.* **34**, 206–213.

KHARIK, V.M. & PLETNER, Y.D. 1990*a* The problem of gravity-gyroscopic waves, which are excited by the oscillations of a curve. *J. Math. Phys.* **31**, 1280–1283.

KHARIK, V.M. & PLETNER, Y.D. 1990*b* The problem of gravity-gyroscopic waves, which are excited by the oscillations of a curve. *J. Math. Phys.* **31**, 1422–1425.

KING, B., ZHANG, H.P. & SWINNEY, H.L. 2009 Tidal flow over three-dimensional topography in a stratified fluid. *Phys. Fluids* **21**, 116601.

KISTOVICH, Y.V. & CHASHECHKIN, Y.D. 2001 Some exactly solvable problems of the radiation of three-dimensional periodic internal waves. *J. Appl. Mech. Tech. Phys.* **42**, 228–236.

KOROBKIN, A.A. 1990 Motion of a body in anisotropic fluid. *Arch. Mech.* **42**, 627–638.

KORPUSOV, M.O., PLETNER, Y.D. & SVESHNIKOV, A.G. 1997*a* On the solvability of an initial-boundary value problem for the internal-wave equation. *Comp. Maths Math. Phys.* **37**, 602–605.

KORPUSOV, M.O., PLETNER, Y.D. & SVESHNIKOV, A.G. 1997*b* Oscillation of a two-sided line segment in a stratified fluid. *Comp. Maths Math. Phys.* **37**, 936–942.

KORPUSOV, M.O., PLETNER, Y.D. & SVESHNIKOV, A.G. 1997*c* Unsteady waves in a stratified fluid excited by the variation of the normal velocity component on a line segment. *Comp. Maths Math. Phys.* **37**, 1076–1085.

KORPUSOV, M.O., PLETNER, Y.D. & SVESHNIKOV, A.G. 1998 Oscillation of a set of curvilinear segments in a stratified fluid. *Comp. Maths Math. Phys.* **38**, 1519–1526.

KRISHNA, D.V. & SARMA, L.V. 1969 Motion of an axisymmetric body in a rotating stratified fluid confined between two parallel planes. *J. Fluid Mech.* **38**, 833–842.

KRUTITSKII, P.A. 1988 Small non-stationary vibrations of vertical plates in a channel with a stratified liquid. *USSR Comp. Maths Math. Phys.* **28** (6), 166–176.

KRUTITSKII, P.A. 1992*a* An explicit solution of the Dirichlet problem for an equation of composite type in a multiply connected domain. *Dokl. Maths* **46**, 63–69.

KRUTITSKII, P.A. 1992*b* Solution of a hyperbolic boundary value problem as a result of applying the principle of limiting amplitude to an initial-boundary value problem for an equation of composite type. *Dokl. Maths* **46**, 118–125.

KRUTITSKII, P.A. 1994 The limit amplitude of the initial and boundary-value problem for an equation of composite type in a multiply connected domain. *Comp. Maths Math. Phys.* **34**, 951–957.

KRUTITSKII, P.A. 1995 An explicit solution of the pseudo-hyperbolic initial boundary value problem in a multiply connected region. *Math. Meth. Appl. Sci.* **18**, 897–925; Erratum. *Math. Meth. Appl. Sci.* **19**, 253 (1996).

KRUTITSKII, P.A. 1996*a* The second initial-boundary-value problem for the gravitational-gyroscopic wave equation. *Comp. Maths Math. Phys.* **36**, 113–123.

KRUTITSKII, P.A. 1996*b* Asymptotics of the gradient of the solution and the inception of singularities in the initial-boundary problem for an equation of a composite type. *Dokl. Maths* **54**, 912–917.

KRUTITSKII, P.A. 1996*c* The second initial boundary value problem for the gravitation-gyroscopic wave equation in exterior domains. *Math. Notes* **60**, 29–41.

KRUTITSKII, P.A. 1996*d* Reduction of the second initial-boundary value problem for the equation of gravitational-gyroscopic waves to a uniquely solvable integral equation. *Differ. Equ.* **32**, 1383–1392.

KRUTITSKII, P.A. 1996*e* An initial-boundary value problem for the evolutionary PDE of composite type with the mixed boundary condition. *Appl. Anal.* **61**, 209–217.

KRUTITSKII, P.A. 1997*a* The first initial-boundary value problem for the gravity-inertia wave equation in a multiply connected domain. *Comp. Maths Math. Phys.* **37**, 113–123.

KRUTITSKII, P.A. 1997*b* The pseudohyperbolic problem arising in the dynamics of stratified rotating fluids. *Appl. Maths Lett.* **10** (2), 117–122.

KRUTITSKII, P.A. 1997*c* An initial-boundary value problem for the pseudo-hyperbolic equation of gravity-gyroscopic waves. *J. Maths Kyoto Univ.* **37**, 343–365.

KRUTITSKII, P.A. 1998 Exterior initial-boundary value problem for a certain evolution equation in a multiply connected domain. *Differ. Equ.* **34**, 1629–1638.

KRUTITSKII, P.A. 2000 The first initial boundary value problem for a compound type equation in a three-dimensional multiply connected region. *Math. Notes* **68**, 217–231.

KRUTITSKII, P.A. 2001 Evolutionary equation of inertial waves in 3-D multiply connected domain with Dirichlet boundary condition. *Intl J. Maths Math. Sci.* **25**, 587–602.

KRUTITSKII, P.A. 2003*a* The jump problem for the equation of internal waves in a stratified rotating fluid. In *Progress in Analysis* (ed. H.G.W. Begehr, R.P. Gilbert & M.W. Wong), vol. 2, pp. 1185–1195. World Scientific.

KRUTITSKII, P.A. 2003*b* Initial-boundary value problem for an equation of internal gravity waves in a 3-D multiply connected domain with Dirichlet boundary condition. *Adv. Maths* **177**, 208–226.

LAI, R.Y.S. & LEE, C.-M. 1981 Added mass of a spheroid oscillating in a linearly stratified fluid. *Intl J. Engng Sci.* **19**, 1411–1420.

LAMB, H. 1932 *Hydrodynamics*, 6th edn. Cambridge University Press.

LANDAU, L.D. & LIFSHITZ, E.M. 1984 *Electrodynamics of Continuous Media*, 2nd edn. Pergamon.

LARSEN, L.H. 1969 Oscillations of a neutrally buoyant sphere in a stratified fluid. *Deep-Sea Res.* **16**, 587–603.

LE DIZÈS, S. & LE BARS, M. 2017 Internal shear layers from librating objects. *J. Fluid Mech.* **826**, 653–675.

LEGENDRE, A.M. 1806 Analyse des triangles tracés sur la surface d'un sphéroïde. *Mém. Cl. Sci. Math. Phys. Inst. Fr.* 1er semestre, 130–161.

LIGHTHILL, J. 1978 *Waves in Fluids*. Cambridge University Press.

LIGHTHILL, J. 1986 *An Informal Introduction to Theoretical Fluid Mechanics*. Oxford University Press.

LLEWELLYN SMITH, S.G. & YOUNG, W.R. 2003 Tidal conversion at a very steep ridge. *J. Fluid Mech.* **495**, 175–191.

MACHICOANE, N., CORTET, P.-P., VOISIN, B. & MOISY, F. 2015 Influence of the multipole order of the source on the decay of an inertial wave beam in a rotating fluid. *Phys. Fluids* **27**, 066602.

MAKAROV, S.A., NEKLYUDOV, V.I. & CHASHECHKIN, Y.D. 1990 Spatial structure of two-dimensional monochromatic internal-wave beams in an exponentially stratified liquid. *Izv. Atmos. Ocean. Phys.* **26**, 548–554.

MARTIN, P.A. 2006 *Multiple Scattering*. Cambridge University Press.

MARTIN, P.A. & LLEWELLYN SMITH, S.G. 2011 Generation of internal gravity waves by an oscillating horizontal disc. *Proc. R. Soc. Lond.* A **467**, 3406–3423.

MARTIN, P.A. & LLEWELLYN SMITH, S.G. 2012 Internal gravity waves, boundary integral equations and radiation conditions. *Wave Motion* **49**, 427–444.

MATHUR, M., CARTER, G.S. & PEACOCK, T. 2014 Topographic scattering of the low-mode internal tide in the deep ocean. *J. Geophys. Res. Oceans* **119**, 2165–2182.

MCLAREN, T.I., PIERCE, A.D., FOHL, T. & MURPHY, B.L. 1973 An investigation of internal gravity waves generated by a buoyantly rising fluid in a stratified medium. *J. Fluid Mech.* **57**, 229–240.

MILNE-THOMSON, L.M. 1968 *Theoretical Hydrodynamics*, 5th edn. Dover.

MIROPOL'SKII, Y.Z. 1978 Self-similar solutions of the Cauchy problem for internal waves in an unbounded fluid. *Izv. Atmos. Ocean. Phys.* **14**, 673–679.

MORSE, P.M. & FESHBACH, H. 1953 *Methods of Theoretical Physics. Part II*. Feshbach Publishing.

MOWBRAY, D.E. & RARITY, B.S.H. 1967 A theoretical and experimental investigation of the phase configuration of internal waves of small amplitude in a density stratified liquid. *J. Fluid Mech.* **28**, 1–16.

MUSGRAVE, R.C., PINKEL, R., MACKINNON, J.A., MAZLOFF, M.R. & YOUNG, W.R. 2016 Stratified tidal flow over a tall ridge above and below the turning latitude. *J. Fluid Mech.* **793**, 933–957.

NYCANDER, J. 2006 Tidal generation of internal waves from a periodic array of steep ridges. *J. Fluid Mech.* **567**, 415–432.

OLVER, F.W.J., LOZIER, D.W., BOISVERT, R.F. & CLARK, C.W. 2010 *NIST Handbook of Mathematical Functions*. NIST/Cambridge University Press.

PEACOCK, T., ECHEVERRI, P. & BALMFORTH, N.J. 2008 An experimental investigation of internal tide generation by two-dimensional topography. *J. Phys. Oceanogr.* **38**, 235–242.

PÉTRÉLIS, F., LLEWELLYN SMITH, S. & YOUNG, W.R. 2006 Tidal conversion at a submarine ridge. *J. Phys. Oceanogr.* **36**, 1053–1071.

PIERCE, A.D. 1963 Propagation of acoustic-gravity waves from a small source above the ground in an isothermal atmosphere. *J. Acoust. Soc. Am.* **35**, 1798–1807.

PIERCE, A.D. 2019 *Acoustics*, 3rd edn. Springer.

PLETNER, Y.D. 1988 Gyroscopic gravitational waves caused by the oscillations of a straight section. *USSR Comp. Maths Math. Phys.* **28** (2), 139–145.

PLETNER, Y.D. 1990*a* On the vibrations of a two-sided disc in a stratified fluid. *USSR Comp. Maths Math. Phys.* **30** (1), 203–212.

PLETNER, Y.D. 1990*b* Vibrations of a flat disk at the interface between two stratified liquids. *USSR Comp. Maths Math. Phys.* **30** (3), 70–80.

PLETNER, Y.D. 1991 The fundamental solution of the equation of internal waves and some initial-boundary value problems. *Comp. Maths Math. Phys.* **31** (4), 79–88.

PLETNER, Y.D. 1992 Fundamental solutions of Sobolev-type operators and some initial boundary-value problems. *Comp. Maths Math. Phys.* **32**, 1715–1728.

PLETNER, Y.D. & TVERSKAYA, L.V. 1989 The problem of the vibrations of a rotating stratified liquid excited by a planar disc. *USSR Comp. Maths Math. Phys.* **29** (2), 94–99.

PLETNER, Y.D. & TVERSKAYA, L.V. 1991 On the problem of the oscillations of a rotating stratified fluid excited by a plane two-sided disc. *Comp. Maths Math. Phys.* **31** (5), 76–83.

POZRIKIDIS, C. 1992 *Boundary Integral and Singularity Methods for Linearized Viscous Flow*. Cambridge University Press.

POZRIKIDIS, C. 2002 *A Practical Guide to Boundary Elements Methods with the Software Library BEMLIB*. Chapman and Hall/CRC.

RIEUTORD, M., GEORGEOT, B. & VALDETARRO, L. 2001 Inertial waves in a rotating spherical shell: attractors and asymptotic spectrum. *J. Fluid Mech.* **435**, 103–144.

RIEUTORD, M. & NOUI, K. 1999 On the analogy between gravity modes and inertial modes in spherical geometry. *Eur. Phys. J.* B **9**, 731–738.

ROBINSON, R.M. 1969 The effects of a vertical barrier on internal waves. *Deep-Sea Res.* **16**, 421–429.

ROBINSON, R.M. 1970 The effects of a corner on a propagating internal gravity wave. *J. Fluid Mech.* **42**, 257–267.

SARMA, L.V.K.V. & KRISHNA, D.V. 1972 Oscillation of axisymmetric bodies in a stratified fluid. *Zastosow. Matem.* **13**, 109–121.

SCHWARTZ, L. 1966 *Mathematics for the Physical Sciences*. Hermann.

SIMAKOV, S.T. 1989 On the small vibrations of a stratified capillary liquid. *J. Appl. Maths Mech.* **53**, 50–56.

SKAZKA, V.V. 1981 Asymptotic estimates for $t \to \infty$ of mixed problems for an equation of mathematical physics. *Siber. Math. J.* **22**, 95–106.

SOBOLEV, S.L. 1954 On a new problem of mathematical physics. *Izv. Akad. Nauk SSSR Ser. Mat.* **18**, 3–50 [in Russian]; English translation in *Selected Works of S.L. Sobolev* (ed. G.V. Demidenko & V.L. Vaskevich), vol. 1, pp. 279–332. Springer (2006).

SOMMERVILLE, D.M.Y. 1933 *Analytical Conics*, 3rd edn. Bell and Sons.

STEWARTSON, K. 1952 On the slow motion of a sphere along the axis of a rotating fluid. *Proc. Camb. Phil. Soc.* **48**, 168–177.

STUROVA, I.V. 2001 Oscillations of a circular cylinder in a linearly stratified fluid. *Fluid Dyn.* **36**, 478–488.

STUROVA, I.V. 2006 Oscillations of a cylinder piercing a linearly stratified fluid layer. *Fluid Dyn.* **41**, 619–628.

STUROVA, I.V. 2011 Hydrodynamic loads acting on an oscillating cylinder submerged in a stratified fluid with ice cover. *J. Appl. Mech. Tech. Phys.* **52**, 415–426.

SUNDUKOVA, A.V. 1991 Fundamental solution of the gravitational-gyroscopic wave equation and the solvability of the internal and external Dirichlet problems. *Comp. Maths Math. Phys.* **31** (10), 87–93.

SUTHERLAND, B.R., DALZIEL, S.B., HUGHES, G.O. & LINDEN, P.F. 1999 Visualization and measurement of internal waves by 'synthetic schlieren'. Part 1. Vertically oscillating cylinder. *J. Fluid Mech.* **390**, 93–126.

SUTHERLAND, B.R. & LINDEN, P.F. 2002 Internal wave excitation by a vertically oscillating elliptical cylinder. *Phys. Fluids* **14**, 721–731.

SVESHNIKOV, A.G., SHISHMAREV, I.A. & PLETNER, Y.D. 1989 Sergei Aleksandrovich Gabov (24.05.1948–19.04.1989). *Vestn. Moskov. Univ. Ser. 3 Fiz. Astron.* (5), 92–93 [in Russian].

VOISIN, B. 1991 Internal wave generation in uniformly stratified fluids. Part 1. Green's function and point sources. *J. Fluid Mech.* **231**, 439–480.

VOISIN, B. 2003 Limit states of internal wave beams. *J. Fluid Mech.* **496**, 243–293.

VOISIN, B. 2009 Added mass in density-stratified fluids. In *Actes du 19ème Congrès Français de Mécanique* (ed. C. Rey, P. Bontoux & A. Chrisochoos). Available at http://hdl.handle.net/2042/37312.

VOISIN, B. 2020 Near-field internal wave beams in two dimensions. *J. Fluid Mech.* **900**, A3.

VOISIN, B., ERMANYUK, E.V. & FLÓR, J.-B. 2011 Internal wave generation by oscillation of a sphere, with application to internal tides. *J. Fluid Mech.* **666**, 308–357.

WATSON, G.N. 1944 *A Treatise on the Theory of Bessel Functions*, 2nd edn. Cambridge University Press.

ZHANG, H.P., KING, B. & SWINNEY, H.L. 2007 Experimental study of internal gravity waves generated by supercritical topography. *Phys. Fluids* **19**, 096602.